PAPER • OPEN ACCESS

Alfvén eigenmode-driven zonal modes saturate and heat thermal ions by cross-scale interactions

To cite this article: Qinghao Yan and P.H. Diamond 2025 *Nucl. Fusion* **65** 116034

OPEN ACCESS
IOP Publishing | International Atomic Energy Agency
Nuclear Fusion
Nucl. Fusion **65** (2025) 116034 (14pp)
https://doi.org/10.1088/1741-4326/ae11c6

Alfvén eigenmode-driven zonal modes saturate and heat thermal ions by cross-scale interactions

Qinghao Yan[1,*] **and P.H. Diamond**[2]

[1] Center for Fusion Sciences, Southwestern Institute of Physics, Chengdu, Sichuan 610041, China
[2] Department of Astronomy and Astrophysics and Department of Physics, University of California San Diego, La Jolla, CA 92093, United States of America

E-mail: qinghaoyan@outlook.com

Received 5 March 2025, revised 24 September 2025
Accepted for publication 10 October 2025
Published 24 October 2025

Abstract

In scenarios where a sustained energetic particle source strongly drives toroidal Alfvén eigenmodes (TAE), and phase-space transport is insufficient to saturate TAE, this novel theory of TAE-zonal mode (ZM)-turbulence—self-regulated by cross-scale interactions (including collisionless ZF damping) – merits consideration. Zonal modes are driven by Reynolds and Maxwell stresses, without the onset of modulational instability. TAE evolution in the presence of ZMs conserves energy and closes the system feedback loop. The saturated zonal shears can be sufficient to suppress ambient drift-ion temperature gradient (ITG) turbulence, achieving an enhanced core confinement regime. The saturated state is regulated by linear and turbulent zonal flow drag. This regulation leads to bursty TAE spectral oscillations, which overshoot while approaching saturation. Heating by both collisional and collisionless ZM damping deposits alpha particle energy into the thermal plasma, achieving effective alpha channeling. This theory offers a mechanism for EP-induced transport barrier formation, and predicts a novel thermal ion heating mechanism.

Keywords: energetic particles, TAE, zonal flow, turbulence, ITB, cross-scale interactions

(Some figures may appear in colour only in the online journal)

1. Introduction

Energetic particles (EPs) are known to excite instabilities such as toroidal Alfvén eigenmodes (TAEs) and energetic particle modes (EPM), potentially leading to significant EP transport and thus affecting fusion plasma confinement [1]. However, recent experiments yielded results that contradict this expectation, showing that EP can be associated with *improved thermal plasma confinement*, through the formation of internal transport barriers (ITBs) [2–6]. These findings highlight discrepancies between experimental results and previous theoretical predictions for EP physics. In addition, conventional turbulent transport models do not account for the effect of EP on thermal confinement. To address these discrepancies, mechanisms have been proposed, such as fast particle dilution [7, 8], electromagnetic stabilization [9] and zonal mode (ZM) stabilization [10–13]. ZM can address two key problems: the saturation of EP-driven instabilities via ZM [4, 14] to prevent strong EP transport and the suppression of turbulence by sheared ZM [15] to form a transport barrier. The TAE/ZM system is an ideal framework for studying these issues. TAE can spontaneously generate ZM via modulational instability, which requires a threshold TAE amplitude [16]. Conversely, the directly driven (forced-driven) process [14, 17–21] does

* Author to whom any correspondence should be addressed.

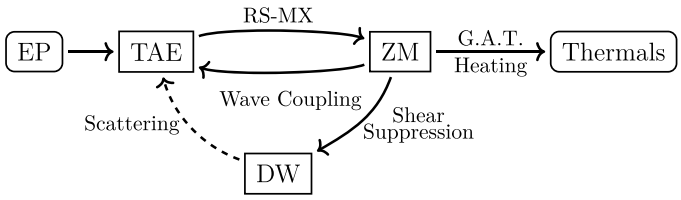

Figure 1. A feedback diagram for TAE and ZM with energy deposition from EP to thermals. TAEs directly drive the evolution of the ZM through RS-MX stresses, while the ZM appears in the TAE evolution equation as a wave-coupling term, ensuring energy conservation and influencing the saturation process of the TAE. The GAT process acts as a collisionless damping mechanism for the ZM, in which the thermal plasma damps the ZM and is thereby heated. The saturated ZM can generate $E\times B$ shearing to suppress DW turbulence. Meanwhile, DW can potentially scatter TAE as mentioned in [27].

not require a threshold TAE amplitude. The nonlinear cross-transport in fusion plasma has been studied in [11, 22–26], but these studies lack saturation mechanism for the directly driven process, especially the proper mechanisms for ZM collisionless damping. The scenario of ZM drive by waves is a well-known paradigm for pattern and structure formation, such as atmospheric jets, Jovian bands and drift wave-zonal flow (DW-ZF) turbulence in tokamaks. Here, the new element is the presence of *two* wave populations—the TAEs and DWs—which couple via the ZM.

As we will show in this paper, with the sustained EP profile and strongly excited TAE, the interactions between TAEs and directly driven ZM lead to an interesting self-organized state of the system, which arises from the feedback loop structure as shown in figure 1: ZM is directly driven by TAE via Reynolds and Maxwell stresses, and damped by collisional and collisionless drag processes. This, in turn, influences the evolution of the TAE via wave-ZM interaction. ZM damping regulates the TAE saturation level and the oscillations of TAE and ZM as they approach saturation. The geodesic acoustic transference (GAT) is a relevant collisionless damping mechanism, which requires sufficient turbulent mixing to be effective. GAT heats ions nonlinearly, ultimately functioning as an alpha channeling process. EP transport is connected to thermal turbulence by cross-scale interactions. The shearing effect from the saturated ZM can be sufficient to suppress DW turbulence, leading to a transport barrier for thermals.

The remainder of this paper is organized as follows. Section 2 introduces the predator–prey model arising from the interaction between TAE and ZM. Section 3 discusses the geodesic acoustic transference as a collisionless damping mechanism for the ZM. Section 4 presents the saturation dynamics of TAE and ZM, along with the associated heating of thermal ions via ZM damping. Finally, section 5 concludes this paper.

2. Predator–prey model for TAE and ZM

To investigate the feedback interactions between TAE and ZM, we use $\delta\phi$ and $\delta A_\parallel$ for scalar potential and parallel vector potential respectively, and define $\delta L\equiv\delta\phi-(v_\parallel\delta A_\parallel/c)$, $\delta\psi\equiv\delta A_\parallel\omega/(ck_\parallel)$. Following the notations in [18, 19], let $\delta\phi=\delta\phi_Z+\delta\phi_T$, where $\delta\phi_Z$ is the zonal component and $\delta\phi_T\equiv\delta\phi_0+\delta\phi_{0*}$, with $\delta\phi_0$ and $\delta\phi_{0*}$ having the opposite real frequencies. Therefore, a collision of two counter-propagating eigenmodes is considered here. Using the ballooning decomposition in (r,θ,ϕ), we have

$$\delta\phi_0=\hat{A}_0e^{i\int\hat{k}_{r,0}\mathrm{d}r+i(n\phi-m_0\theta-\omega_0t)}\sum_j e^{-ij\theta}\Phi_0(x-j)$$
$$\delta\phi_Z=\hat{A}_Ze^{i\int\hat{k}_Z\mathrm{d}r-i\omega_Zt}\sum_m\Phi_Z$$

where Φ_0 above accounts for the fine scale structure of TAE, $\hat{A}_0$ is the envelope amplitude, and $\hat{k}_{r,0}$ stands for the radial envelope wave number. From the gyrokinetic nonlinear vorticity equation [1, 18, 19, 28], one can obtain the nonlinear evolution of TAE $\delta\phi_0$ as equation (1):

$$\begin{aligned}&-k_\parallel^2\delta\psi_0+\frac{\omega_0^2}{V_A^2}\delta\phi_0=\frac{4\pi\omega_0 e}{c^2k_{\perp,0}^2}\langle J_{k_0}\omega_d\delta H_{k_0}\rangle_{\mathcal{E}}\\&-i\frac{c}{B_0}\frac{k_Zk_{\theta,0}}{k_{\perp,0}^2}\left(k_Z^2-k_{\perp,0}^2\right)\frac{\omega_0}{V_A^2}\delta\phi_0(\delta\phi_Z-\delta\psi_Z)\end{aligned}\tag{1}$$

where $\mathcal{E}\equiv v^2/2$, $\mathbf{k}\delta\phi=[k_\parallel\hat{b}+k_\theta\hat{\theta}+(\hat{k}_r-inq'\partial_x\ln\Phi)\hat{r}]\delta\phi$, $V_A^{-2}\equiv4\pi n_0e^2\rho_i^2/(c^2T_i)$, ρ_i is the ion Lamour radius, $J_k=J_0(k_\perp\rho_L)$ is the Bessel function, EP distribution function is decomposed as equilibrium and fluctuating parts $F=F_0+\delta H$. The ZM contributions are the second term on the rhs. The breaking of the ideal magnetohydrodynamics (MHD) condition is expressed as:

$$\delta\phi_0-\delta\psi_0=i\frac{c}{B_0}\frac{k_\theta k_Z}{\omega_0}(\delta\psi_Z-\delta\phi_Z)\delta\phi_0.\tag{2}$$

In equation (1), the integral $\langle\cdots\rangle_{\mathcal{E}}\equiv\int\sqrt{\mathcal{E}}\mathrm{d}\mathcal{E}$ of the fast particle distribution δH appears. This is obtained from the nonlinear gyrokinetic equation [29]:

$$\begin{aligned}&\left(-i\omega+v_\parallel\partial_l+i\omega_d+\Omega_Z\right)\delta H_k=\\&\quad-i\frac{e_s}{m}Q_0F_0J_k\delta L_k-\frac{c}{B_0}\Lambda_kJ_{k'}\delta L_{k'}\delta H_{k''}\end{aligned}\tag{3}$$

where $\Lambda_k\equiv\sum_{k=k'+k''}\hat{b}\cdot\mathbf{k}''\times\mathbf{k}'$. Then, the 'linear' response to the TAE mode $\delta\phi_0$ is written as [30, 31]:

$$\delta H_0^L=-\frac{e}{m}Q_0F_0e^{i\lambda_{d0}}J_{k_0}\delta L_0\sum_l\frac{(-1)^lJ_l\left(\hat{\lambda}_{d0}\right)e^{il(\theta-\theta_0)}}{\omega_0-k_{\parallel,0}v_\parallel-l\omega_t-i\Omega_Z}\tag{4}$$

where $\omega_d = \hat{v}_{d,\mathcal{E}}(k_r \sin\theta + k_\theta \cos\theta)$, $\hat{v}_{d,\mathcal{E}} = (v_\perp^2 + 2v_\parallel^2)/(2\Omega_i R_0)$, $Q_0 F_0 \equiv (\omega_0 \partial_\mathcal{E} - \omega_*)F_0$, $\omega_* F_0 = \mathbf{k}\cdot\mathbf{b}\times\nabla F_0/\Omega_i$, $L_{n0E}^{-1} \equiv -\mathrm{d}\ln n_{0E}/\mathrm{d}r$, Ω_i is the thermal ion cyclotron frequency, $\Omega_Z \equiv ck_{\theta,0}k_Z J_Z \delta L_Z/B_0 \simeq k_{\theta,0}V_{E\times B}$ is the nonlinear phase shift from ZM, $\lambda_{d0} = \hat{\lambda}_{d0}\sin(\theta-\theta_0)$, $\hat{\lambda}_{d0} = k_{\perp,0}\hat{\rho}_{d,\mathcal{E}}$, $\hat{\rho}_{d,\mathcal{E}} = qR_0\hat{v}_{d,\mathcal{E}}/v_\parallel$, $\tan\theta_0 = k_r/k_\theta$, $J_l(\hat{\lambda}_{d0})$ is the l-th order Bessel function of $\hat{\lambda}_{d0}$. For large parallel velocity, there is $\omega_t = v_\parallel/qR_0$.

Multiplying equation (1) by $\delta\phi_{0*}$, utilizing equations (2) and (4), and assuming a slowing down distribution function $F_{0E} = n_{0E}\mathcal{E}^{-3/2}/\ln(\mathcal{E}_f/\mathcal{E}_c)$ with $\mathcal{E}_c \leqslant \mathcal{E} \leqslant \mathcal{E}_f$ and $\mathcal{E}_f = v_f^2/2$ ($\mathcal{E}_f$ is the maximum fast particle energy, $\mathcal{E}_c$ is the critical energy below which the slowing-down approximation is no longer valid), we obtain the evolution equation for $|\delta\phi_0|^2$ or, equivalently, a wave kinetic equation. This is as follows (see appendix A.1 for more details):

$$\begin{aligned}&\left(1-\frac{k_{\parallel,0}^2V_A^2}{\omega_0^2}\right)\partial_t|\delta\phi_0|^2\\ &=\left(1-\frac{k_{\parallel,0}V_A}{\omega_0}\right)\frac{\omega_A\pi}{2\sigma}q^3k_{\theta,0}\rho_A\beta_E f_r\frac{R_0}{L_{n0E}}|\delta\phi_0|^2\\ &\quad-\left(1-\frac{k_Z^2}{k_{\perp,0}^2}-\frac{k_{\parallel,0}^2V_A^2}{\omega_0^2}\right)\frac{2c}{B_0}k_{\theta,0}k_Z|\delta\phi_0|^2\delta\phi_Z.\end{aligned}\tag{5}$$

Here we have only considered $l=\pm1$ transit resonances, $\omega_A \equiv V_A/(qR_0)$, $\rho_A \equiv V_A/\Omega_i$, $\beta_E \equiv 8\pi n_{0E}m_i\mathcal{E}_f/B_0^2$, $\sigma \equiv \ln(\mathcal{E}_f/\mathcal{E}_c)\mathcal{E}_f/V_A^2$, f_r is a factor related to the fraction of resonant particles [30]. We neglected zonal current (ZC, $\delta\psi_Z$) here, since ZC primarily brings additional magnetic shear to the system, which should have a small effect on TAE evolution [10, 16, 19, 20]. Equation (5) consists of the usual linear growth from the wave-particle resonance (rhs term $\propto|\delta\phi_0|^2$) [30, 31], and damping from the nonlinear interaction between TAE and ZM (rhs term $\propto|\delta\phi_0|^2\delta\phi_Z$). Therefore, equation (5) can be cast into the form of $\partial_t|\delta\phi_0|^2 = \gamma_L|\delta\phi_0|^2 - \gamma_d|\delta\phi_0|^2\delta\phi_Z$, as equation (12) discussed later.

The evolution equation for ZM is obtained from the zonal components of the gyrokinetic vorticity equation as below [1, 18, 19, 28]:

$$\begin{aligned}&\frac{e^2}{T_i}\left\langle\left(1-J_Z^2\right)F_{0,i}\right\rangle_\mathcal{E}\partial_t\delta\phi_Z = \\ &\qquad-\textstyle\sum_s\langle e_s J_Z i\omega_d\delta H_0\rangle_{\mathcal{E},Z} + (\text{RS-MX})_Z\end{aligned}.\tag{6}$$

On the rhs, the first term is the curvature coupling term (CCT), where the bracket denotes an integral in velocity space followed by zonal-averaging ($\frac{1}{2\pi}\int_{-\pi}^{\pi}\cdots d\theta$). Since $\langle(\cdots)\delta H_0^L\rangle_{\mathcal{E},Z} = 0$ according to the linear EP response equation (4), the CCT can contribute to the ZM only through the nonlinear response of the distribution, i.e. $\langle(\cdots)\delta H_0^{NL}\rangle_{\mathcal{E},Z} \neq 0$[18]. However, as we will show later, as a higher order response, the CCT contribution should be small. The second term accounts for the Reynolds and Maxwell stresses (RS-MX), which are primarily thermal contributions and can be included following [16, 18, 19, 32]. Considering $k_\perp\rho_i \ll 1$ and $k_\perp\hat{\rho}_{d,\mathcal{E}} \ll 1$, we have the evolution of the zonal potential as (see details in appendix A.2):

$$\partial_t\delta\phi_Z = \frac{ck_{\theta,0}\hat{F}}{\hat{\chi}_{iZ}B_0}\left[\frac{n_{0E}\hat{\rho}_{d,f}^2}{n_0\rho_i^2}\hat{G}+\left(1-\frac{k_{\parallel,0}^2V_A^2}{\omega_0^2}\right)\right]|\delta\phi_0|^2\tag{7}$$

where $\hat{\chi}_{iZ} \equiv \chi_{iZ}/(k_Z^2\rho_i^2) \simeq 1.6q^2/\sqrt{\varepsilon}$ is the neoclassical polarizability of ZM [33], $\varepsilon \equiv a/R_0$, $\hat{\rho}_{d,f} \equiv qv_f/\Omega_i$, $\hat{F} \equiv i(k_{r,0} - k_{r,0*})$, $\hat{G}$ is defined as:

$$\begin{aligned}\hat{G} \equiv \Bigg\langle &\Omega_{*E}\frac{F_{0,E}}{2n_{0,E}}\frac{v_{\parallel,\mathcal{E}}^2}{v_f^2}\left(1-\frac{k_\parallel v_\parallel}{\omega}\right)_0\left(1-\frac{k_\parallel v_\parallel}{\omega}\right)_{0*}\\ &\times\sum_{l=\pm1}\frac{-i}{\omega_0 - k_{\parallel,0}v_\parallel - l\omega_t - i\Omega_Z}\Bigg\rangle_\mathcal{E}\end{aligned}\tag{8}$$

where we defined $\Omega_{*E} \equiv k_\theta L_{n_{0E}}^{-1}cT_i/eB$ to separate the energy dependence in the integral, and $\hat{\omega}_{*E} \equiv \Omega_{*E}T_E/T_i$. The two parts in the rectangle bracket on the rhs of equation (7) originate from CCT ($\propto\hat{G}$) and RS-MX (in round brackets), respectively. We corrected the results from [18, 19], and found that CCT is equivalent to a turbulent stress like RS-MX. They share similar structures:

1. Both are proportional to the TAE amplitude $|\delta\phi_0|^2$ and $\hat{F}$, indicating that the collision of two TAEs and the asymmetry in their mode structures are essential for ZM generation. Notably, this property was not identified for the CCT in reference [18, 19].
2. Both exhibit polarization effects, either from gyro-motion (ρ_i^2) or EP drift ($\hat{\rho}_{d,f}^2$). Notice that both sides of equation (7) are divided by ρ_i^2.
3. Both require the breaking of ideal MHD condition $1 - (k_{\parallel,0}^2V_A^2/\omega_0^2) \sim \varepsilon \neq 0$. For CCT, this factor arises from the integral of $\hat{G}$.

Compared to [18, 19], the corrected expression for $\hat{G}$ reveals the necessity of a breaking of the ideal MHD condition, showing that $\hat{G} \propto \varepsilon$. The importance of $\hat{F}$ is now recognized for the CCT contribution too. Because not every portion in EP density is at resonant, the resonant particle density $n_{E,R} = f_r n_{0E}$ with $f_r < 1$ [30]. Therefore, we have $\hat{G} \propto \varepsilon f_r|\Omega_{*E}/\omega_0|$. Then, the ratio of CCT to RS-MX can be written as $\mathcal{O}(n_{E,R}\hat{\omega}_{*E}q^2/(n_0\omega_0))$, which is different from [19] by a $1/\varepsilon$ factor (originate from the breaking of ideal MHD condition in $\hat{G}$). Typically, there is $\hat{\omega}_{*E}/\omega_0 \gg 1$. However, the resonant particle density is also small, $n_{E,R}/n_0 \ll 1$, which makes it hard to estimate the ratio of CCT to RS-MX. Thus, we rewrite the ratio as:

$$\frac{\text{CCT}}{\text{RS-MX}} \sim \frac{f_r n_{0E}}{n_0}\frac{\hat{\rho}_{d,f}^2}{\rho_i^2}\left|\frac{\Omega_{*E}}{\omega_0}\right| \sim f_r q^2\frac{P_E}{P_i}\left|\frac{\Omega_{*E}}{\omega_0}\right| \ll 1\tag{9}$$

for the strongly driven scenario $f_\beta \equiv P_E/P_i \sim 1$, $q \sim 1$ and $|\Omega_{*E}/\omega_0| < 1$, where $P_E = n_{0E}T_E$, $P_i = n_0T_i$, $T_E \equiv m_i\mathcal{E}_f$. Consequently, RS-MX predominantly drives the generation of

ZM. A detailed comparison using realistic device parameters is provided in appendix A.2.

Another issue in retaining CCT [18, 19] as a ZF drive source is the necessity of a corresponding ***sink*** to ensure the energy conservation. As we mentioned early, CCT contribute to ZM via the *nonlinear* EP response. Therefore, the possible corresponding 'sink' in other evolution equations should originate from δH_0^{NL} too and eventually manifest in the EP distribution. However, there is no such 'sink' explicitly in other evolution equations to balance the energy that CCT transfers to ZM. Given that the contribution of CCT is secondary and that energy conservation is essential, we omit the CCT in equation (7) and later cast it in the form of $\partial_t \delta\phi_Z = \gamma_2|\delta\phi_0|^2 + \cdots$, which is equation (13).

Using a quasi-linear approach, we can estimate the effects of TAE on the EP distribution [34, 35]. Then, the evolution equation of the EP profile, accounting for external EP sources such as neutral beam heating or ion cyclotron resonance heating, is formally written as below (see appendix A.3 for details):

$$\partial_t n_{0E} = -D_{\rm res}\hat{F}L_{n_{0E}}^{-1} n_{0E} + \text{Source} + \cdots \tag{10}$$

where the TAE transport coefficient is:

$$D_{\rm res} \simeq \frac{\pi}{2\sigma}\frac{k_Z^2\hat{\rho}_{d,f}^2 V_A f_r}{k_{\parallel,0}}\left(\frac{\delta B_r}{B_0}\right)^2. \tag{11}$$

Now we can simplify the evolution of TAE and ZM, neglecting CCT, and rewriting equations (5) and (7) as equations (12) and (13):

$$\partial_t|\delta\phi_0|^2 = \gamma_1|\delta\phi_0|^2 - \gamma_d|\delta\phi_0|^2\delta\phi_Z \tag{12}$$

$$\hat{\chi}_{iZ}\partial_t\delta\phi_Z = \gamma_2|\delta\phi_0|^2 - \nu\delta\phi_Z \tag{13}$$

where,

$$\gamma_1 \equiv \frac{\pi\omega_A}{2\sigma}q^3 k_{\theta,0}\rho_A\beta_E f_r\frac{R_0}{L_{n0E}}$$

$$\gamma_d \equiv \frac{2c}{B_0}k_{\theta,0}k_Z, \quad \gamma_2 \equiv \frac{c}{B_0}k_{\theta,0}\hat{F}\varepsilon$$

$\nu = (\nu_{ii} + \nu_G)$ is the damping of ZM. ν_{ii} is the ion-ion collisional damping [33, 36] and ν_G stands for possible collisionless damping. Here, ν is caused by interactions in thermal plasma; therefore, it will not affect the calculation of EP-driven TAEs. Equations (10)–(13) constitute a system describing the dynamics of EP, TAE and ZM. Note that for $\varepsilon\hat{F}/\hat{\chi}_{iZ} = k_Z$, the RS-MX terms cancel perfectly upon addition of the evolution equation for TAE and ZM amplitude (i.e. $\partial_t(|\delta\phi_0|^2 + |\delta\phi_Z|^2) = \gamma_1|\delta\phi_0|^2 - \nu|\delta\phi_Z|^2/(2\hat{\chi}_{iZ})$)! This reflects energy conservation. This system is similar to the well-known 'Predator-Prey' system [15, 17, 36], as shown in figure 1. Here, we focus on the cases where the EP profile is sustained by external sources, the continuum damping is negligible and the wave-particle trapping is unable to saturate the TAE ($\gamma_1/\omega_0 > 10^{-2}$, see equation (4.176) in [1]). In essence, *this system is not near marginal*. Hence, we further simplify the system by hereafter ignoring the evolution equation (10) for EP. This simplified system manifests a closed feedback loop, featuring a robust EP source, strongly excited TAEs, and ZM generation through RS-MX. Subsequently, the ZM is damped and feeds back to the evolution of TAE through the nonlinear wave-ZM interaction, leading to the saturation in both TAE and ZM. Assuming γ_1, γ_2, γ_d and ν are constants, the saturation levels are straightforwardly obtained as below, showing that the saturation of TAE is controlled by the damping of ZM

$$(\delta\phi_Z)_S = \gamma_1/\gamma_d \tag{14}$$

$$\left(|\delta\phi_0|^2\right)_S = \gamma_1\nu/\left(\gamma_d\gamma_2\right). \tag{15}$$

3. Collisionless ZM damping

When only collisional damping is present and as $\nu = \nu_{ii} \to 0$, the TAE saturation level decreases, accompanied by intense oscillations in both TAE and ZM, as shown in figure 2. The oscillation frequency can be easily obtained from equations (12) and (13) as $f_{\rm osc} \sim \sqrt{\nu\gamma_1}/\omega_A$ when $\nu \lesssim 4\gamma_1$. This can appear as an intermittent (bursty) signal of TAE prior to saturation, and differs fundamentally from the quasi-periodic chirping caused by profile relaxation [11, 37, 38]. Furthermore, this property emphasizes the crucial role of collisionless ZM damping.

Considering the significant oscillation of ZM when $\nu_{ii} \to 0$, which can drive thermal ion and electron oscillations in space, we introduce a simple mechanism for collisionless ZM damping, namely the geodesic acoustic transference [39–41]. According to [39–41], due to the variation of the toroidal magnetic field in the radial direction, the $E \times B$ flow is stronger on the low field side than on the high field side. The divergence of $E \times B$ flow and compressional work lead to a pressure sideband with sinusoidal structure $p_s \propto \sin\vartheta$ in the poloidal direction ϑ. The result is an oscillation between the zonal field and $m = 1, n = 0$ pressure side band, which can be expressed as:

$$\partial_t\langle\tilde{u}\rangle_Z = \cdots - \omega_B\langle p_s\sin\vartheta\rangle_Z \tag{16}$$

where $\omega_B \equiv 2L_\perp/R$. The background gradient of the thermal profile is defined in the negative radial direction $L_\perp \equiv -p_e\nabla r/\nabla p_e$, $\tilde{u}$ is the fluctuating $E \times B$ flow in the poloidal direction, $\langle\tilde{u}\rangle_Z$ is the zonal flow, which can be expressed as $ik_Z\delta\phi_Z c/B_0$ then normalized by factor $C_S qR/L_\perp$, where $C_S \equiv T_e/M_i$. Time is normalized by factor $C_S/L_\perp$. The energy in the pressure sideband couples to thermal particles, mostly via turbulent mixing and dissipation of the parallel current [41]. In the collisionless regime, resistivity should be weak, making turbulent mixing the dominant process. The evolution of the electron pressure sideband can be expressed as:

$$\partial_t\langle p_{e,s}\sin\vartheta\rangle_Z = -\tau_{\rm turb}^{-1}\langle p_{e,s}\sin\vartheta\rangle_Z + \frac{\omega_B}{2}\langle\tilde{u}\rangle_Z. \tag{17}$$

Here, magnetic flutter effects and ion flow sideband are neglected, defining $\tau_{\rm turb}^{-1} \equiv D_{\rm turb}/L_\perp^2$. A quasilinear turbulent coefficient $D_{\rm turb} \simeq {\rm Re}\sum_{\tilde{\mathbf{k}}} i\frac{c^2}{B_0^2}|\phi_{\tilde{\mathbf{k}}}|^2/(\omega - \tilde{\mathbf{k}}_\perp\cdot\mathbf{v}_E)$ is assumed, with $\tilde{\mathbf{k}}_\perp$ representing the wave number of the thermal turbulence and $\mathbf{v}_E$ denotes $E \times B$ advection. The resonance of the thermal

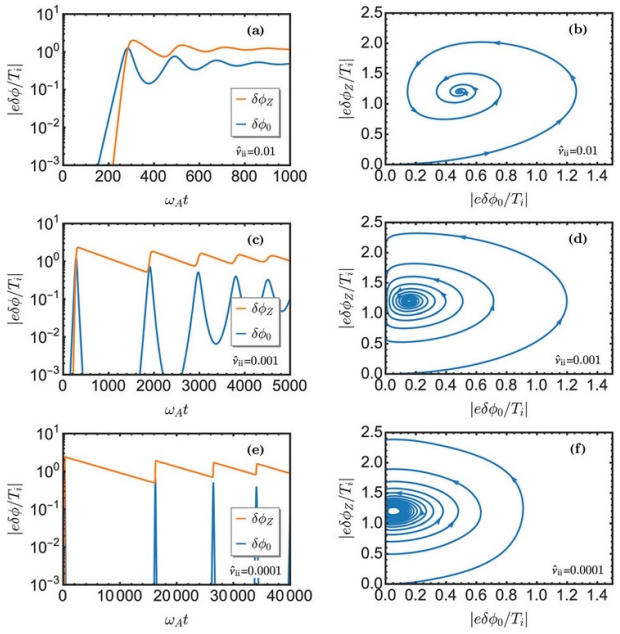

Figure 2. (*a*), (*c*), (*e*): TAE $\delta\phi_0$ and zonal potential $\delta\phi_Z$ evolve to the fixed points in: (*b*), (*d*), (*f*). ZM collisional damping rate $\hat{\nu}_{ii} \equiv \nu_{ii}/(\hat{\chi}_{iZ}\omega_A)$ is decreased from top to bottom. γ_1, γ_2 and γ_d are the same as in figure 3.

particle turbulence with zonal $E \times B$ flows gives the irreversibility which underpins the turbulent mixing. When $L_\perp/R \ll 1$, thermal turbulence has sufficient time (on the order of $\sim L_\perp/C_S$) to respond to changes in the pressure sideband induced by geodesic acoustic oscillations, which evolve on the timescale $\sim R/C_S$. Moreover, as mentioned earlier, in the case of TAE-driven ZM under a collisionless regime ($\nu \to 0$), the ZM oscillation timescale is $1/f_{\rm osc} \sim \omega_A/\sqrt{\nu\gamma_1} \to \infty$, which is even slower-therefore allowing enough time for thermal turbulence to respond.

Dedimensionalizing equations (12), (13) and (17) yields equation (18)–(20), respectively. Geodesic acoustic coupling appears as the third term on the rhs of equation (19) (see appendix B for details)

$$\partial_\tau x = \hat{\gamma}_1 x - \hat{\gamma}_d xy \tag{18}$$

$$\partial_\tau y = \hat{\gamma}_2 x - \hat{\nu}_{ii} y - \hat{\gamma}_{G1} z \tag{19}$$

$$\partial_\tau z = \hat{\gamma}_{G2} y - \left(\omega_A \tau_{\rm turb}\right)^{-1} z. \tag{20}$$

Here $\tau \equiv \omega_A t$, $x \equiv |e\delta\phi_0/T_i|^2$, $y \equiv e\delta\phi_Z/T_i$, $z \equiv (1+\tau_i)\langle \hat{p}_{e,s} \sin\vartheta\rangle_Z$, $\tau_i \equiv T_i/T_e$, $\hat{p}_{e,s}$ is the electron pressure sideband normalized to equilibrium pressure. Coefficients are dedimensionlized:

$$\hat{\gamma}_1 \equiv \frac{\gamma_1}{\omega_A}, \quad \hat{\gamma}_d \equiv \frac{2D_B k_{\theta,0} k_Z}{\omega_A}, \quad \hat{\gamma}_2 = \frac{\hat{\gamma}_d}{2}, \quad \hat{\nu}_{ii} \equiv \frac{\nu_{ii}}{\hat{\chi}_{iZ}\omega_A},$$

$$\hat{\gamma}_{G1} \equiv \frac{C_S^2 q R_0 \omega_B}{ik_Z D_B \hat{\chi}_{iZ}\omega_A L_\perp^2}, \quad \hat{\gamma}_{G2} \equiv (1+\tau_i)\frac{ik_Z D_B}{V_A}\frac{\omega_B}{2}$$

where $D_B \equiv cT_i/(eB_0)$ and $\varepsilon\hat{F}/\hat{\chi}_{iZ} = k_Z$ is applied. It's easy to find the geodesic acoustic oscillation from $\hat{\gamma}_{G1}\hat{\gamma}_{G2} = \omega_{\rm GAM}^2/(\hat{\chi}_{iZ}\omega_A^2)$, where $\omega_{\rm GAM}^2 \equiv 2(1+\tau_i)C_S^2/R^2$ is the geodesic acoustic mode (GAM) frequency. The GAT can provide an extra damping of the ZM, which is obtained from the static sideband $z_{\rm static} = \hat{\gamma}_{G2}\omega_A\tau_{\rm turb} y$ and $\hat{\gamma}_{G1} z_{\rm static}$ as:

$$\hat{\nu}_G = \frac{1}{\hat{\chi}_{iZ}}\frac{\omega_{\rm GAM}^2}{\omega_A \tau_{\rm turb}^{-1}} \sim \mathcal{O}\left(10^{-2}\right) - \mathcal{O}\left(10^{-1}\right). \tag{21}$$

Note that turbulent mixing ($\tau_{\rm turb}$) is necessary for collisionless ZM damping here. When compared to $\hat{\nu}_{ii} \leqslant \mathcal{O}(10^{-4})$, collisionless damping from GAT will be dominant.

4. Saturation of TAE and ZM

The saturation of TAE. Specifically, using $k_Z^2\rho_i^2 \lesssim k_\perp^2\rho_i^2 \sim \varepsilon^2$ and $k_\parallel = 1/(2qR_0)$, we obtain the saturation level of TAE from equation (15) as:

$$\left(\frac{\delta B_r}{B_0}\right)_S^2 \sim \frac{\pi q^2}{4\sigma\hat{\chi}_{iZ}\varepsilon^2}\frac{\beta_E f_r k_{\theta,0}}{L_{n0E}}\frac{\nu\rho_i^2}{\Omega_i}. \tag{22}$$

This is directly proportional to the damping of ZM, akin to the case in the DW-ZF system [15, 36]. Equation (21) demonstrates that turbulence can regulate the saturation of TAE through the ZM damping. In addition, if EP transport is governed by TAE, since $\hat{\nu}_G \propto \tau_{\rm turb}$, then *as turbulence increases (indicated by the decrease in τ_{turb}), the EP transport coefficient will decrease*. However, as we will discuss latter, the shearing feedback of ZM on turbulence will modify this straightforward conclusion. This behavior suggests interesting cross-scale interactions between EP and thermal turbulence.

Introducing $\tau_Z^{-1} \equiv D_B k_{\theta,0} k_Z$, we notice that when $3\hat{\gamma}_d\hat{\gamma}_2 \sim (\omega_A\tau_{\rm turb})^{-2}$ or $\tau_Z \sim \tau_{\rm turb}$, the system will oscillate at the frequency of $\omega_{\rm GAM}$ rather than $f_{\rm osc}$, which is similar to the results in [20]. This can be understood from the perspective of the energy flow of the system: EP $\xrightarrow{\gamma_1}$ TAE $\xrightarrow{\tau_Z^{-1}}$ ZM $\xrightarrow{\rm GAT}$ p_s $\xrightarrow{\tau_{\rm turb}^{-1}}$ Turbulence. The condition $\tau_Z \sim \tau_{\rm turb}$ indicates that the energy drained by ZM from the TAE is equal to the energy dissipated by the pressure sideband. As a result, if the EP is sustained (i.e. γ_1 is a constant) the energy transfer will be controlled by the GAT, leading to oscillations at $\omega_{\rm GAM}$. To generate such oscillations, we use the Bohm coefficient $D_{\rm turb} = D_B/16$ and $(\rho_i/L_\perp)^2 \sim 0.02$ in the subsequent analyses, ensuring $\tau_Z \sim \tau_{\rm turb}$ and $1/(\omega_A\tau_{\rm turb}) \ll 1$. For typical parameters in tokamaks like DIII-D with $q = 1.5$, $\sigma \sim 2.5$, $\beta_E = 1\%$, $f_r = 0.25$, $k_{\theta,0} = nq/a \sim 10$, $L_{n0E} = 0.5a$, we have $\hat{\gamma}_1 \sim 0.12$, $\hat{\gamma}_d \sim 0.1$, $\hat{\gamma}_2 \sim 0.05$, $\hat{\nu}_G \sim 0.1$, $\hat{\gamma}_{G1} \sim -3.9i$, $\hat{\gamma}_{G2} \sim 0.0012i$, $1/(\omega_A\tau_{\rm turb}) \sim 0.045$ (see appendix C for more details), then the evolution of the system is shown in figure 3, which closely resembles figure 10 in [20]. The saturated TAE amplitude we obtained is $(\delta B_r/B_0)_S^2 \sim 10^{-7}$. Comparing this to the threshold for spontaneous generation $\rho_i^2/(4\varepsilon(qR_0)^2)$ [16], yields a ratio of ${\rm TAE}_{\rm sat/th} \sim \mathcal{O}(10^{-1}) - \mathcal{O}(1)$. This suggests that spontaneous generation is possible after the directly driven process saturates. A similar process is found for ITG turbulence simulation [42–44], where eigenmode self-interaction [45] dominates ZF generation, and the modulation of sidebands [46] becomes important only near nonlinear saturation. The estimated EP transport coefficient using

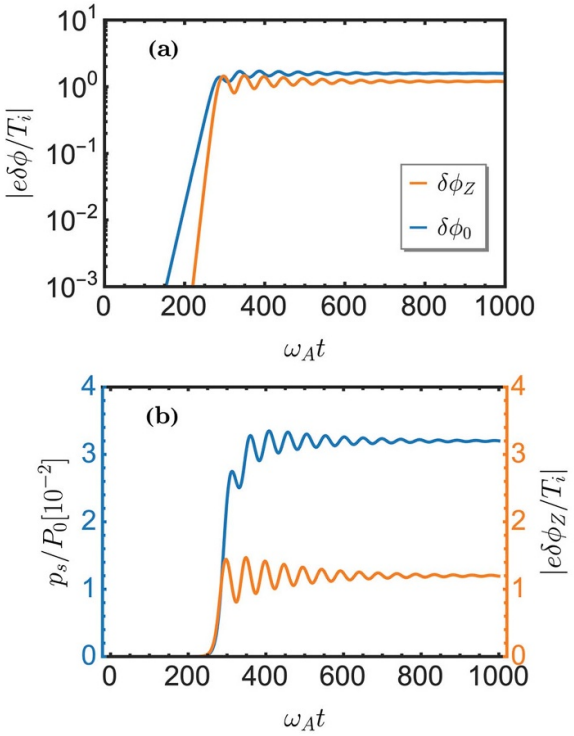

Figure 3. The evolution of TAE-ZM system with the geodesic acoustic transference as collisionless damping. The collisional damping rate is $\hat{\nu}_{ii} = 10^{-5}$, the effective collisionless damping rate is $\hat{\nu}_G = 10^{-1}$. Oscillations with frequency of $\omega_{\rm GAM}$ are observed when $\tau_Z \sim \tau_{\rm turb}$.

equation (11) is around $D_{\rm res} \sim \mathcal{O}(10)\ {\rm m}^2\ {\rm s}^{-1}$, which exceeds the neoclassical value but is limited, and so does not cause severe EP transport. This also facilitates the maintenance of a sustained EP profile through modulated heating, to align with the assumption of a fixed linear TAE growth rate.

The saturation of ZM. The saturation level of the zonal potential can be estimated from equation (14) as:

$$(\delta\phi_Z)_S \sim \frac{\pi}{2\sigma}\frac{T_i}{e}\frac{f_\beta f_r q^2}{k_Z L_{n0E}}. \tag{23}$$

Then the ZF shear $\omega_{E\times B} \equiv ck_Z^2\delta\phi_Z/B_0$ is:

$$\omega_{E\times B} = \frac{\pi}{2\sigma}q^2 D_B f_\beta f_r \frac{k_Z}{L_{n_{0E}}} \sim \frac{\pi}{2\sigma}q^2\varepsilon f_\beta f_r \frac{C_S}{L_{n_{0E}}}. \tag{24}$$

The radial scale of ZM k_Z is crucial in determining the saturation levels. Factors such as the fraction of EP pressure f_β, the fraction of resonant particles f_r and the EP gradient $L_{n_{0E}}^{-1}$ also influence the strength of ZF [12]. For the typical parameters mentioned previously, the ZF shear reaches around $0.3C_S/a$ in regions where TAEs are excited, a magnitude comparable to the ITG linear growth rate with a dilution effect $\gamma_{\rm ITG} \sim 0.1C_S/a$ [47, 48]. Therefore, the suppression of ITG turbulent transport can be anticipated. The threshold condition for shear suppression, $\omega_{E\times B} > \gamma_{\rm ITG}$, translates into a criterion for the TAE linear growth rate $\gamma_{\rm TAE} = \gamma_1/2 > \gamma_{\rm ITG}k_{\theta,0}/k_Z$. This criterion further implies a threshold for the strength of the EP source (e.g. from neutral beam injection heating). There may appear to be a conflict concerning strong ZF shearing and necessary turbulence for ZM damping. However, since ZM damping occurs via a pressure sideband, in a strongly (weakly) turbulent state, the pressure sideband weakens (strengthens), resulting in strong (weak) ZM and shearing, and consequently facilitating reduction (enhancement) of turbulence. Moreover, when $\tau_Z \sim \tau_{\rm turb}$, the GAM plays a role in dissipating EP energy in this system. In general, zonal shears do affect DW and consequently regulate TAE, a process not explored in this paper. This interaction could result in a dynamical $\hat{\nu}_G$ and thereby influence EP transport.

The $E\times B$ velocity caused by ZF can be estimated as:

$$V_{E\times B} \sim \frac{\pi}{2\sigma}q^2 f_\beta f_r \frac{C_S\rho_i}{L_{n_{0E}}}. \tag{25}$$

The heating power transferred from EP to thermals, estimated from equation (13) as $\nu_G V_{E\times B}^2$ in steady state, can be distributed to both ions and electrons ($\tau_i \sim 1$) or predominately into electrons ($\tau_i \ll 1$). The ZF phase shift (Ω_Z) in equation (4) is smaller than the transit frequency (ω_t) by roughly two orders of magnitude. Thus, Ω_Z affects near marginal transit resonance or trapped particle dynamics [14, 29]. Modulation of wave-particle resonance by ZF could lead to mesoscopic structure such as the $E\times B$ staircase [49, 50]. Additionally, a thermal ion ITB produced by ZF shearing will likely drive substantial bulk ion intrinsic rotation [51–54].

5. Conclusions

This work introduces a novel Predator-Prey type theory for the collective dynamics of EP, TAE, turbulence and ZM, which highlights the crucial role of collisionless ZM damping and predicts a novel alpha channeling mechanism. This work presents a theoretical explanation for ITB formation driven by EPs through directly driven ZM, and a new explanation of bursty TAE phenomena. Experiments from JET have indicated the existence of TAE-driven ZM [4, 6, 55]. Our results may contribute to the development of a novel operational scenario in future fusion devices like ITER. Other collisionless ZM damping mechanisms, such as the resonant diffusion of the zonal vorticity itself [56], are also noteworthy. The effective Richardson number is ${\rm Ri} \sim (\gamma_1/\omega_{E\times B})^2 \sim (k_{\theta,0}/k_Z)^2$ and $0.25 < {\rm Ri} \lesssim 0.5$, suggests that the K-H instability is unlikely to damp ZM for the parameters considered here [57, 58].

We assume a sustained EP drive to eliminate EP profile relaxation, which is a reasonable strategy for isolating the key new physics—the saturation of AE via collisionless ZM damping. When the system is near-marginal, the interplay between the ZF shift, wave-particle trapping [59–61] and stochastic scattering [27, 62–64] is also interesting. This model is relevant to scenarios without significant phase-space transport, characterized by the absence of complex mode chirping and overlap in the spectrum. Without ZM, our model would lead to unbounded TAE growth. The most direct correction is to consider the growth rate feedback from profile flattening or by phase-space relaxation in the future. The effective EP phase

space gradient reconstruction rate $\nu_{\rm eff} \approx \nu_\perp \omega_A/\omega_b$ [37] with wave trapping frequency $\omega_b \propto \sqrt{\phi_{\rm AE}}$, increases as the AE saturation amplitude decreases in the presence of ZM [20, 21, 24, 25]. Therefore, we anticipate a faster recovery of the EP phase space structure when ZMs are included in the simulation. In addition, turbulence may also have an effect on decorrelating EP phase-space clumps and holes [65]. Our model can serve as a basis for understanding these issues in the future. Finally, this work explores novel cross-scale interactions in fusion plasmas, introducing a compelling mechanism for transferring EP energy to thermal ions via ZM, while facilitating the formation of a TAE-driven ITB to enhance thermal confinement.

Acknowledgments

We thank Ruirui Ma, Michael Fitzgerald, T. S. Hahm, Gyungjin Choi, Xiaodi Du and Wei Chen for useful discussions. This work was supported by the National Key R&D Program of China under Grant No. 2022YFE03100004 and National Science Foundation of China Grant No.12175053, U.S. DOE, Office of Science, under Award Number DE-FG02-04ER54738. The authors would like to thank the Isaac Newton Institute for Mathematical Sciences, Cambridge, for support and hospitality during the Program 'Anti-diffusive Dynamics: from Sub-Cellular to Astrophysical Scales', where part of the work on this paper was undertaken. This work was supported by EPSRC Grant EP/R014604/1.

Appendix A. Model derivation

A.1. TAE evolution

The gyrokinetic nonlinear vorticity equation is [1, 18, 28]:

$$
\begin{aligned}
&-i\frac{c^2B_0}{4\pi\,\omega_k}\partial_l\left(\frac{k_\perp^2}{B}\right)\partial_l\delta\psi_k+\frac{e^2}{T_i}\left\langle\left(1-J_k^2\right)F_{0,i}\right\rangle_{\mathcal{E}}\partial_t\delta\phi_k\\
&\quad=-\sum_s\left\langle e_sJ_k i\omega_d\delta H\right\rangle_{\mathcal{E}}-\frac{c\Lambda_k}{B_0}\left[\frac{c^2k_\perp^{\prime\prime2}\partial_l\delta\psi_{k'}\partial_l\delta\psi_{k''}}{4\pi\,\omega_{k'}\omega_{k''}}\right.\\
&\qquad\left.+\left\langle e\left(J_kJ_{k'}-J_{k''}\right)\delta L_{k'}\delta H_{k''}\right\rangle\right].
\end{aligned}
\tag{A1}
$$

From equation (A1), one can obtain the TAE evolution as represented by equation (1). Applying equation (2), the evolution of TAE amplitude is:

$$
\begin{aligned}
\left(1-\frac{k_{\parallel,0}^2V_A^2}{\omega_0^2}\right)\partial_t|\delta\phi_0|^2&=-2\frac{4\pi eV_A^2}{c^2k_{\perp,0}^2}\left\langle J_{k_0}i\omega_d\delta H\right\rangle_{\mathcal{E}}\delta\phi_{0*}\\
&-\left(1-\frac{k_Z^2}{k_{\perp,0}^2}-\frac{k_{\parallel,0}^2V_A^2}{\omega_0^2}\right)\frac{2c}{B_0}k_{\theta,0}k_Z|\delta\phi_0|^2\delta\phi_Z.
\end{aligned}
\tag{A2}
$$

Using the linear response equation (4), and notice the push-forward operator should result in the factor $e^{-i\hat{\lambda}_{d0}\sin(\theta-\theta_0)}=\sum_l(-1)^lJ_l(\hat{\lambda}_{d0})e^{il(\theta-\theta_0)}$, the particle resonance drive for TAE is:

$$
\begin{aligned}
&\left\langle J_{k_0}i\omega_d\delta H_k^L\right\rangle_{\mathcal{E}}\\
&\quad=-\left\langle\frac{e}{m}J_{k_0}^2\delta L_0Q_0F_{0E}i\hat{v}_{d,\mathcal{E}}k_{\perp,0}\sum_l\frac{(-1)^lJ_l\left(\hat{\lambda}_{d0}\right)}{\omega_0-k_\parallel v_\parallel-l\omega_{\rm t}}\right.\\
&\qquad\left.\times\frac{1}{2\pi}\int{\rm d}\theta\cos\left(\theta-\theta_0\right)e^{il(\theta-\theta_0)}e^{i\hat{\lambda}_{d0}\sin(\theta-\theta_0)}\right\rangle_{\mathcal{E}}\\
&\quad\simeq\left\langle\frac{e}{m}\delta L_0Q_0F_{0E}\hat{v}_{d,\mathcal{E}}\hat{\rho}_{d,\mathcal{E}}\frac{k_{\perp,0}^2}{4}\sum_{l=\pm1}\frac{i{\rm sign}\left(l\right)}{\omega_0-k_\parallel v_\parallel-l\omega_{\rm t}}\right\rangle_{\mathcal{E}}
\end{aligned}
$$

where we have used

$$
\begin{aligned}
&\frac{1}{2\pi}\int{\rm d}\theta\cos\left(\theta-\theta_0\right)e^{il(\theta-\theta_0)}e^{i\hat{\lambda}_{d0}\sin(\theta-\theta_0)}\\
&\quad=\frac{1}{4\pi}\int{\rm d}\theta\left[e^{i(l+1)(\theta-\theta_0)}+e^{i(l-1)(\theta-\theta_0)}\right]e^{i\hat{\lambda}_{d0}\sin(\theta-\theta_0)}\\
&\quad=\frac{1}{2}\left[J_{-l-1}\left(\hat{\lambda}_{d0}\right)+J_{-l+1}\left(\hat{\lambda}_{d0}\right)\right]
\end{aligned}
$$

and only $l=\pm1$ transit resonance are considered. Notice $J_{-l}(a)=(-1)^lJ_l(a)$, $k_\perp\rho_L\ll1$ and $k_\perp\rho_{d,\mathcal{E}}\ll1$, $J_{k_0}=J_0(k_{\perp,0}\rho_L)\simeq1$, $J_1(\hat{\lambda}_{d0})\simeq\frac{\hat{\lambda}_{d0}}{2}$, $J_2(\hat{\lambda}_{d0})\simeq\frac{\hat{\lambda}_{d0}^2}{8}$, $\hat{\lambda}_{d0}=k_{\perp,0}\hat{\rho}_{d,\mathcal{E}}$.

For large parallel velocity, we have $v_\parallel\simeq\sqrt{\mathcal{E}}$ and

$$
\delta L_0=\delta\phi_0-\frac{v_\parallel}{c}\delta A_{\parallel,0}\simeq\delta\phi_0\left(1-\frac{k_{\parallel,0}v_\parallel}{\omega_0}\right).
$$

Then,

$$
\begin{aligned}
\left\langle J_{k_0}i\omega_d\delta H_k^L\right\rangle_{\mathcal{E}}&=\delta\phi_0\frac{k_{\perp,0}^2}{4}\frac{e}{m}\frac{qn_{0E}}{R_0\Omega_i^2}\left\langle\left(1-\frac{\sqrt{\mathcal{E}}k_{\parallel,0}}{\omega_0}\right)\right.\\
&\left.\times\left(\omega_0\partial_{\mathcal{E}}+\frac{k_\theta}{\Omega_iL_{n_{0E}}}\right)\frac{F_{0E}}{n_{0E}}\sum_{l=\pm1}\frac{i\mathcal{E}^{3/2}{\rm sign}\left(l\right)}{\omega_0-\left(k_\parallel+\frac{l}{qR_0}\right)\sqrt{\mathcal{E}}}\right\rangle_{\mathcal{E}}.
\end{aligned}
$$

Assuming the slowing down distribution $F_{0E}=n_{0E}\mathcal{E}^{-3/2}/\ln(\mathcal{E}_f/\mathcal{E}_c)$, then the energy integral will be:

$$
\begin{aligned}
&\int\left(1-\frac{\sqrt{\mathcal{E}}k_{\parallel,0}}{\omega_0}\right)\left(\omega_0\partial_{\mathcal{E}}+\frac{k_\theta}{\Omega_iL_{n_{0E}}}\right)\frac{1}{\ln\left(\mathcal{E}_f/\mathcal{E}_c\right)}\\
&\qquad\times\sum_{l=\pm1}\frac{i\mathcal{E}^{1/2}{\rm d}\mathcal{E}{\rm sign}\left(l\right)}{\omega_0-\left(k_\parallel+\frac{l}{qR_0}\right)\sqrt{\mathcal{E}}}\\
&\quad\simeq\left(1-\frac{k_{\parallel,0}V_A}{\omega_0}\right)\frac{1}{\ln\left(\mathcal{E}_f/\mathcal{E}_c\right)}\frac{k_\theta}{\Omega_iL_{n_{0E}}}\\
&\qquad\times\sum_{l=\pm1}i{\rm sign}\left(l\right)\left[\frac{2\omega_0^2}{\left(k_\parallel+\frac{l}{qR_0}\right)^3}\ln\frac{1-\frac{\sqrt{\mathcal{E}_c}\left(k_\parallel+\frac{l}{qR_0}\right)}{\omega_0}}{1-\frac{\sqrt{\mathcal{E}_f}\left(k_\parallel+\frac{l}{qR_0}\right)}{\omega_0}}\right.\\
&\qquad\left.+\frac{2\omega_0^2\left(\sqrt{\mathcal{E}_c}-\sqrt{\mathcal{E}_f}\right)}{\left(k_\parallel+\frac{l}{qR_0}\right)^2}+\frac{\omega_0\left(\mathcal{E}_c-\mathcal{E}_f\right)}{k_\parallel+\frac{l}{qR_0}}\right].
\end{aligned}
$$

Assuming there is $\mathcal{E}_f \gtrsim V_A \gg \mathcal{E}_c$ and $\gamma_L \ll \omega_{0R}$, then the real part is given by:

$$\left(1-\frac{k_{\parallel,0}V_A}{\omega_0}\right)\frac{1}{\ln(\mathcal{E}_f/\mathcal{E}_c)}\frac{k_{\theta,0}}{\Omega_i L_{n_{0E}}} \times \sum_{l=\pm1} i\frac{-2\omega_0^2 \mathrm{sign}(l)}{\left(k_\parallel+\frac{l}{qR_0}\right)^3} i\Im \ln\left[1-\frac{\sqrt{\mathcal{E}_f}\left(k_\parallel+\frac{l}{qR_0}\right)}{\omega_0}\right] = -\left(1-\frac{k_{\parallel,0}V_A}{\omega_0}\right)\frac{1}{\ln(\mathcal{E}_f/\mathcal{E}_c)}\frac{k_{\theta,0}}{\Omega_i L_{n_{0E}}} \times \sum_{l=\pm1}\frac{2\omega_0^2\mathrm{sign}(l)}{\left(k_\parallel+\frac{l}{qR_0}\right)^3} ii\,(-\pi)\,\mathrm{Heav}\left(\frac{\sqrt{\mathcal{E}_f}\left(k_\parallel+\frac{l}{qR_0}\right)}{\omega_0}-1\right) = -\left(1-\frac{k_{\parallel,0}V_A}{\omega_0}\right)\frac{1}{\ln(\mathcal{E}_f/\mathcal{E}_c)}\frac{2\pi k_{\theta,0}V_A^3}{|\omega_0|\Omega_i L_{n_{0E}}} \times \left[\mathrm{Heav}\left(\frac{\sqrt{\mathcal{E}_f}}{V_A}-1\right)+\frac{1}{9}\mathrm{Heav}\left(\frac{3\sqrt{\mathcal{E}_f}}{V_A}-1\right)\right]$$

where $\mathrm{Heav}(x)$ is the Heaviside Theta function, which is 0 for $x<0$ and 1 for $x\geqslant 0$. Finally, there is:

$$\frac{4\pi e V_A^2}{c^2 k_{\perp,0}^2}\delta\phi_{0*}\times\delta\phi_0\frac{k_{\perp,0}^2}{4}\frac{e}{m}\frac{qn_{0E}}{R_0\Omega_i^2}\times(-)\times\left(1-\frac{k_{\parallel,0}V_A}{\omega_0}\right) \times\frac{1}{\ln(\mathcal{E}_f/\mathcal{E}_c)}\frac{2\pi k_\theta V_A^3}{|\omega_0|\Omega_i L_{n_{0E}}} = -\left(1-\frac{k_{\parallel,0}V_A}{\omega_0}\right) \times|\delta\phi_0|^2\frac{\pi\omega_A q^3 k_{\theta,0}\rho_A\beta_E}{4\ln(\mathcal{E}_f/\mathcal{E}_c)\mathcal{E}_f/V_A^2}\frac{R_0}{L_{n0E}}$$

where $V_A^{-2}\equiv 4\pi n_0 e^2\rho_i^2/(c^2T_i)=4\pi\rho_m/B_0^2$, $\omega_A\equiv V_A/qR_0$, $\beta_E\equiv 8\pi n_{0E}m_i\mathcal{E}_f/B_0^2$, $\rho_A\equiv V_A/\Omega_i$. Putting it back into the TAE amplitude evolution gives equation (5) as:

$$\left(1-\frac{k_{\parallel,0}^2V_A^2}{\omega_0^2}\right)\partial_t|\delta\phi_0|^2=\left(1-\frac{k_{\parallel,0}V_A}{\omega_0}\right)\frac{\omega_A\pi}{2\sigma} \times q^3k_{\theta,0}\rho_A\beta_E f_r\frac{R_0}{L_{n0E}}|\delta\phi_0|^2 -\left(1-\frac{k_Z^2}{k_{\perp,0}^2}-\frac{k_{\parallel,0}^2V_A^2}{\omega_0^2}\right)\frac{2c}{B_0}k_{\theta,0}k_Z|\delta\phi_0|^2\delta\phi_Z \tag{A3}$$

where $\sigma\equiv\ln(\mathcal{E}_f/\mathcal{E}_c)\mathcal{E}_f/V_A^2$. A factor related to the fraction of resonant particles f_r is added. Assuming $(1-\frac{k_\parallel^2V_A^2}{\omega_0^2})\sim\varepsilon$, $(k_Z/k_{\perp,0})^2\ll 1$, then we can have:

$$\partial_t|\delta\phi_0|^2=\gamma_1|\delta\phi_0|^2-\gamma_d|\delta\phi_0|^2\delta\phi_Z \tag{A4}$$

where

$$\gamma_1\equiv\frac{\pi\omega_A}{2\sigma}q^3k_{\theta,0}\rho_A\beta_E f_r\frac{R_0}{L_{n0E}} \tag{A5}$$

$$\gamma_d\equiv\frac{2c}{B_0}k_{\theta,0}k_Z. \tag{A6}$$

Then the saturation level of ZM is:

$$(\delta\phi_Z)_S=\frac{\gamma_1}{\gamma_d}\simeq\frac{\pi}{2\sigma}\frac{T_i}{e}\frac{q^2f_\beta f_r}{k_Z L_{n0E}} \tag{A7}$$

which is equation (23). Then the $E\times B$ shear is:

$$\omega_{E\times B}\equiv\frac{ck_Z^2}{B_0}\delta\phi_Z=\frac{\pi}{2\sigma}\frac{cT_i}{eB_0}\frac{q^2f_\beta f_r k_Z}{L_{n0E}} \sim\frac{\pi}{2\sigma}\frac{q^2f_\beta f_r}{L_{n0E}}C_S\rho_i\frac{\varepsilon}{\rho_i}=\frac{\pi}{2\sigma}q^2f_\beta f_r\varepsilon\frac{C_S}{L_{n0E}} \tag{A8}$$

which is equation (24), where $k_Z^2\rho_i^2<k_\perp^2\rho_i^2\sim\varepsilon^2$ is used. The threshold condition $\omega_{E\times B}>0.1C_S/a$ gives $f_\beta f_r>0.1(2\sigma L_{n0E})/(\pi\varepsilon q^2 a)\sim 0.1$, for parameters used in the paper. The $E\times B$ velocity is

$$V_{E\times B}=\frac{ck_Z}{B_0}\delta\phi_Z=\frac{\pi}{2\sigma}q^2f_\beta f_r\frac{C_S\rho_i}{L_{n0E}}. \tag{A9}$$

A.2. Zonal mode evolution

From equation (A1), one can obtain the zonal mode evolution as equation (6). The contribution of CCT to ZM evolution is obtained from the nonlinear response [18]:

$$\left(i\omega_d\delta H_0^{NL}\right)_Z\sim-\frac{c}{B_0}\Lambda_Z J_{k'}\delta L_{k'}\delta H_{k'}^L, \tag{A10}$$

where $\Lambda_Z\equiv\sum_{k_Z=k'+k''}\hat{b}\cdot\mathbf{k}''\times\mathbf{k}'$. Then it gives:

$$\left\langle e_i J_Z i\omega_d\delta H_0^{NL}\right\rangle_{\mathcal{E},Z}=\frac{1}{2\pi}\frac{ce}{B_0}\left\langle J_Z\int\mathrm{d}\theta\hat{H}_0\left(J_{k_0}\delta L_0\delta H_{0*}^L - J_{k_{0*}}\delta L_{0*}\delta H_0^L\right)\right\rangle_{\mathcal{E}}.$$

Then

$$J_{k_0}\delta L_0\delta H_{0*}^L=-\frac{e}{m}J_{k_0}J_{k_{0*}}\delta\phi_0\delta\phi_{0*} \times\left(1-\frac{k_\parallel v_\parallel}{\omega}\right)_0\left(1-\frac{k_\parallel v_\parallel}{\omega}\right)_{0*}Q_{0*}F_0 \times\sum_{l*}\frac{(-1)^{l_*}J_{l*}\left(\hat{\lambda}_{d0*}\right)e^{il_*(\theta-\theta_{0*})}e^{i\lambda_{d0*}}}{\omega_{0*}-k_{\parallel,0*}v_\parallel-l_*\omega_t-i\Omega_{Z*}}$$

$$J_{k_{0*}}\delta L_{0*}\delta H_0^L=-\frac{e}{m}J_{k_0}J_{k_{0*}}\delta\phi_0\delta\phi_{0*} \times\left(1-\frac{k_\parallel v_\parallel}{\omega}\right)_0\left(1-\frac{k_\parallel v_\parallel}{\omega}\right)_{0*}Q_0F_0 \times\sum_{l}\frac{(-1)^{l}J_{l}\left(\hat{\lambda}_{d0}\right)e^{il(\theta-\theta_0)}e^{i\lambda_{d0}}}{\omega_0-k_{\parallel,0}v_\parallel-l\omega_t-i\Omega_Z}.$$

Notice $Q_0F_0=(\omega_0\partial_E-\omega_*)F_0=-Q_{0*}F_0$ and $\hat{H}_0\equiv k_{\theta,0}(k_{r,0}+k_{r,0*})=-\hat{H}_{0*}$, $\theta_{0*}\equiv\tanh^{-1}(k_{r,0*}/k_{\theta,0*})$. The sign of CCT should not change when exchange ω_0 and ω_{0*}.

Therefore $l_* = -l$. Using the relations $e^{ia\sin\theta} = \sum_l J_l(a)e^{il\theta}$, $J_{-l}(a) = (-1)^l J_l(a)$, $\lambda_{d0} = \hat{\lambda}_{d0}\sin(\theta-\theta_0)$, we have

$$\begin{aligned}
&\int \mathrm{d}\theta\,(-1)^l J_l\left(\hat{\lambda}_{d0}\right) e^{il(\theta-\theta_0)} e^{i\lambda_{d0}} \\
&\quad = \sum_{l'}\int_{-\pi}^{\pi} \mathrm{d}\theta\,(-1)^l J_l\left(\hat{\lambda}_{d0}\right) J_{l'}\left(\hat{\lambda}_{d0}\right) e^{il(\theta-\theta_0)} e^{il'(\theta-\theta_0)} \\
&\quad = 2\pi\sum_{l'}(-1)^l J_l\left(\hat{\lambda}_{d0}\right) J_{l'}\left(\hat{\lambda}_{d0}\right) e^{-i(l+l')\theta_0}\delta(l_1+l') \\
&\quad = 2\pi\sum_{l} J_l^2\left(\hat{\lambda}_{d0}\right).
\end{aligned}$$

Then recall $k_\perp\rho_L \ll 1$ and $k_\perp\rho_{d,\mathcal{E}} \ll 1$, there is

$$\begin{aligned}
\left\langle e_i J_Z i\omega_d \delta H_0^{NL}\right\rangle_Z &\propto \hat{H}_0\left[J_1^2\left(\hat{\lambda}_0\right) - J_1^2\left(\hat{\lambda}_{0*}\right)\right] \qquad \text{(A11)}\\
&= k_{\theta,0}\hat{\rho}_{d,\mathcal{E}}^2\left(k_{r,0}+k_{r,0*}\right)\left(k_{r,0}^2 - k_{r,0*}^2\right) \\
&= k_{\theta,0}\hat{\rho}_{d,\mathcal{E}}^2\left(k_{r,0}+k_{r,0*}\right)^2\left(k_{r,0}-k_{r,0*}\right) \\
&= -k_{\theta,0}k_Z^2\hat{\rho}_{d,\mathcal{E}}^2 i\hat{F} \qquad \text{(A12)}
\end{aligned}$$

where $\hat{F} \equiv i(\hat{k}_{r,0} - \hat{k}_{r,0*}) + \partial_r \ln\Phi_0 - \partial_r \ln\Phi_{0*}$. Notice above result is a correction on [18]. Putting it back into CCT, we have equation (A13).

$$\left\langle e_i J_Z i\omega_d \delta H_0^{NL}\right\rangle_{\mathcal{E},Z} = \frac{ce^2}{2B_0 m} n_{0E} k_{\theta,0} k_Z^2 \hat{\rho}_{d,f}^2 \hat{F}\hat{G}|\delta\phi_0|^2 \qquad \text{(A13)}$$

where $\hat{\rho}_{d,f} \equiv qv_f/\Omega_i$, $\mathcal{E}_f = v_f^2/2$, $\hat{G}$ is defined as below

$$\begin{aligned}
\hat{G} \equiv \Bigg\langle \Omega_{*E}\frac{F_{0,E}}{2n_{0,E}}\frac{v_{\parallel,\mathcal{E}}^2}{v_f^2}\left(1-\frac{k_\parallel v_\parallel}{\omega}\right)_0\left(1-\frac{k_\parallel v_\parallel}{\omega}\right)_{0*} \\
\times \sum_{l=\pm1}\frac{-i}{\omega_0 - k_{\parallel,0}v_\parallel - l\omega_t - i\Omega_Z}\Bigg\rangle_{\mathcal{E}}
\end{aligned} \qquad \text{(A14)}$$

with $\Omega_{*E} \equiv \dfrac{cT_i}{eB_0}k_\theta L_{n_{0E}}^{-1}$. Meanwhile, the RS-MX contribution to ZM evolution is [16, 19]:

$$\text{RS-MX} = \frac{1}{2}\frac{e^2 c n_0}{T_i B_0} k_{\theta,0} k_Z^2 \rho_i^2 \hat{F}\left(1 - \frac{k_{\parallel,0}^2 V_A^2}{\omega_0^2}\right)|\delta\phi_0|^2. \qquad \text{(A15)}$$

Then the evolution for ZF is:

$$\begin{aligned}
\left\langle\left(1-J_Z^2\right)F_{0,i}\right\rangle_{\mathcal{E}}\partial_t\delta\phi_Z &= \frac{cT_i n_{0E}}{2B_0 m}k_{\theta,0}k_Z^2\hat{\rho}_{d,f}^2\hat{G}\hat{F}|\delta\phi_0|^2 \\
&+ \frac{1}{2}\frac{cn_0}{B_0}k_{\theta,0}k_Z^2\rho_i^2\hat{F}\left(1-\frac{k_{\parallel,0}^2V_A^2}{\omega_0^2}\right)|\delta\phi_0|^2
\end{aligned}$$

which is written as equation (7):

$$\hat{\chi}_{iZ}\partial_t\delta\phi_Z = \frac{c}{B_0}k_{\theta,0}\hat{F}\left[\frac{n_{0E}}{n_0}\frac{\hat{\rho}_{d,f}^2}{\rho_i^2}\hat{G} + \left(1-\frac{k_{\parallel,0}^2V_A^2}{\omega_0^2}\right)\right]|\delta\phi_0|^2$$

where $\left\langle(1-J_Z^2)F_{0,i}\right\rangle_{\mathcal{E}} = \frac{k_Z^2\rho_i^2 n_0}{2}\hat{\chi}_{iZ}$ is used. Notice a factor $1-(k_{\parallel,0}^2V_A^2/\omega_0^2) \sim \varepsilon$ should arise from the integral of $(1-\frac{k_\parallel v_\parallel}{\omega})_0(1-\frac{k_\parallel v_\parallel}{\omega})_{0*}$ in $\hat{G}$ to characterize the breaking of ideal MHD condition. Then there is $\hat{G} \propto \varepsilon f_r|\Omega_{*E}/\omega_0|$ with resonant particle fraction f_r. The resulting ratio between CCT and RS-MX is

$$\begin{aligned}
\frac{\text{CCT}}{\text{RS-MX}} &\sim \frac{f_r n_{0E}}{n_0}\frac{\hat{\rho}_{d,f}^2}{\rho_i^2}\left|\frac{\Omega_{*E}}{\omega_0}\right| \sim f_r q^2\frac{P_E}{P_i}\left|\frac{\Omega_{*E}}{\omega_0}\right| \\
&= q^2\frac{f_r n_{0E}}{n_0}\left|\frac{\hat{\omega}_{*E}}{\omega_0}\right|
\end{aligned}$$

where we defined $\Omega_{*E} \equiv k_\theta L_{n_{0E}}^{-1}\frac{cT_i}{eB}$ and $\hat{\omega}_{*E} \equiv k_\theta L_{n_{0E}}^{-1}\frac{cT_E}{eB} = \Omega_{*E}T_E/T_i$. Notice the last expression above is the same as $\mathcal{O}(n_{E,R}\hat{\omega}_{*E}q^2/(n_0\omega_0\varepsilon))$ obtained in [19] except the ε factor, where we corrected the breaking of ideal MHD condition in $\hat{G}$.

- For parameters state like in DIII-D at half minor radius: $k_\theta = m/r \sim 5/0.25\,\text{m}$, $1/L_{n0E} \sim 1/0.25\,\text{m}$, $T_i = 2\,\text{keV}, B = 2T, q = 1.5, f_r = 0.25, f_\beta = 1$, we have $f_r q^2 f_\beta|\Omega_{*E}/\omega_0| \sim 0.25\times 1.5^2\times\frac{80\,\text{kHz}}{120\,\text{kHz}} = 0.375 < 1$
- For parameters state like in JET at half minor radius: $k_\theta = m/r \sim 5/0.45\,\text{m}$, $1/L_{n0E} \sim 1/0.45\,\text{m}$, $T_i = 4\,\text{keV}, B = 3.7T, q = 1.5, f_r = 0.25, f_\beta = 1$, we have $f_r q^2 f_\beta|\Omega_{*E}/\omega_0| \sim 0.25\times 1.5^2\times\frac{27\,\text{kHz}}{160\,\text{kHz}} \sim 0.1 < 1$

Thus, we conclude that

$$\frac{\text{CCT}}{\text{RS-MX}} \ll 1.$$

Another issue of keeping the CCT as a ZF drive source is we need to have a corresponding ***sink*** in other physics quantities to satisfy the energy conservation. However, there is no explicit 'sink' to supply energy to ZM in [19]. Considering that the contribution of the CCT is secondary and the model needs to conserve energy, we omit the CCT in equation (13) to simplify the model. Then the zonal mode evolution is dominated by RS-MX, and equation (7) can be written as equation (13):

$$\hat{\chi}_{iZ}\partial_t\delta\phi_Z = \gamma_2|\delta\phi_0|^2 - \nu\delta\phi_Z$$

with

$$\gamma_2 \equiv \frac{c}{B_0}k_{\theta,0}\hat{F}\left[\frac{n_{0E}}{n_0}\frac{\hat{\rho}_{d,f}^2}{\rho_i^2}\hat{G} + \left(1-\frac{k_\parallel^2V_A^2}{\omega_0^2}\right)\right] \simeq \frac{c}{B_0}k_{\theta,0}\hat{F}\varepsilon \qquad \text{(A16)}$$

and ν is the damping for zonal mode. The saturation level of TAE is

$$\left(|\delta\phi_0|^2\right)_S = \frac{\gamma_1\nu}{\gamma_d\gamma_2} \simeq \frac{\nu\dfrac{\pi\omega_A}{2\sigma}q^3k_{\theta,0}\rho_A\beta_E f_r\dfrac{R_0}{L_{n0E}}}{2\dfrac{c^2}{B_0^2}k_{\theta,0}^2k_Z\hat{F}\varepsilon}$$

with $\delta B_r = \frac{ck_\theta k_\parallel}{\omega_0}\delta\psi$ and $\hat{F}\varepsilon = k_Z\hat{\chi}_{iZ}$, the saturation level of TAE fluctuating is

$$\left(\frac{\delta B_r^2}{B_0^2}\right)_S = \frac{\pi q^2}{4\sigma\hat{\chi}_{iZ}}\frac{\nu\beta_E f_r k_{\theta,0}}{\Omega_i k_Z^2 L_{n0E}} \tag{A17}$$

$$\sim \frac{\pi q^2}{4\sigma\hat{\chi}_{iZ}\varepsilon^2}\frac{\beta_E f_r k_{\theta,0}}{L_{n0E}}\frac{\nu\rho_i^2}{\Omega_i} \tag{A18}$$

which is equation (22).

A.3. EP profile evolution

In deriving the evolution of the EP distribution, we employ the quasi-linear method:

$$\begin{aligned}
\partial_t F_{0E} &= -\frac{c}{B_0}\Lambda_Z J_{k'}\delta L_{k'}\delta H^L_{k'},\\
&= \frac{ce}{B_0 m}\hat{H}_0 J_{k_0}J_{k_{0*}}\delta L_0\delta L_{0*}Q_0 F_{0E}\\
&\quad\times\left(\sum_{l*}\frac{J^2_{l*}\left(\hat{\lambda}_{d0*}\right)}{\omega_{0*}-k_{\|,0*}v_\|-l_*\omega_t-i\Omega_{Z*}}\right.\\
&\quad\left.+\sum_l\frac{J^2_l\left(\hat{\lambda}_{d0}\right)}{\omega_0-k_{\|,0}v_\|-l\omega_t-i\Omega_Z}\right)\\
&= -\frac{ce}{B_0 m}\hat{H}_0 J_{k_0}J_{k_{0*}}\delta L_0\delta L_{0*}Q_0F_{0E}\times\\
&\quad\sum_{l=\pm1}\frac{J^2_l\left(\hat{\lambda}_{d0}\right)-J^2_l\left(\hat{\lambda}_{d0*}\right)}{\omega_0-k_{\|,0}v_\|-l\omega_t-i\Omega_Z}\\
&= -\frac{ce}{B_0 m}k_{\theta,0}k_Z^2\hat{\rho}^2_{d,\mathcal{E}}\hat{F}J_{k_0}J_{k_{0*}}\delta L_0\delta L_{0*}Q_0F_{0E}\times\\
&\quad\times\sum_{l=\pm1}\frac{-i}{\omega_0-k_{\|,0}v_\|-l\omega_t-i\Omega_Z}.
\end{aligned}$$

Then after integral in $\mathcal{E}$,

$$\partial_t n_{0E} = -\frac{\pi}{2\sigma}\frac{c^2}{B_0^2}\frac{k^2_{\theta,0}k_Z^2\hat{F}\hat{\rho}^2_{d,f}|\delta\phi_0|^2 f_r}{|\omega_0|}L^{-1}_{n_{0E}}n_{0E} \tag{A19}$$

$$= -\frac{\pi}{2\sigma}\frac{k_Z^2\hat{\rho}^2_{d,f}f_r|\omega_0|}{k_\|^2}\left(\frac{\delta B_r}{B_0}\right)^2\hat{F}L^{-1}_{n_{0E}}n_{0E} \tag{A20}$$

$$= \partial_r D_{\rm res}\partial_r n_{0E} \tag{A21}$$

where

$$D_{\rm res} = \left\langle\frac{c^2}{B_0^2}k^2_{\theta,0}k_Z^2\hat{\rho}^2_{d,\mathcal{E}}\delta L_0\delta L_{0*}\frac{F_{0E}}{n_{0E}}\right.$$
$$\left.\times\sum_{l=\pm1}\frac{-i}{\omega_0-k_{\|,0}v_\|-l\omega_t-i\Omega_Z}\right\rangle_\mathcal{E} \tag{A22a}$$

$$D_{\rm res}\simeq\frac{\pi}{2\sigma}\frac{k_Z^2\hat{\rho}^2_{d,f}V_A f_r}{k_{\|,0}}\left(\frac{\delta B_r}{B_0}\right)^2 \tag{A22b}$$

is the equation (11). Then, the evolution of EP profile is:

$$\partial_t n_{0E} = -\gamma_3|\delta\phi_0|^2 n_{0E} + \text{Source} + \cdots \tag{A23}$$

with the external source and coefficient:

$$\gamma_3 = \frac{D_{\rm res}\hat{F}L^{-1}_{n_{0E}}}{|\delta\phi_0|^2}. \tag{A24}$$

Using equation (15), when the supply rate of external EP source exceeds the flatten rate of EP profile below, we can have a sustained EP profile

$$\frac{D_{\rm res}\hat{F}L^{-1}_{n_{0E}}}{\omega_A} = \frac{\pi}{4\sigma}f_r\frac{\hat{F}\hat{\rho}^2_{d,f}}{L_{n0E}}\hat{\nu}\hat{\gamma}_1. \tag{A25}$$

A.4. The evolution diagram of P-P system

Dedimensionlize the equation (12):

$$\partial_t|\delta\phi_0|^2 = \gamma_1|\delta\phi_0|^2 - \gamma_d|\delta\phi_0|^2\delta\phi_Z$$
$$\frac{1}{\omega_A}\partial_t\left|\frac{e\delta\phi_0}{T_i}\right|^2 = \frac{\gamma_1}{\omega_A}\left|\frac{e\delta\phi_0}{T_i}\right|^2 - \frac{\gamma_d}{\omega_A}\frac{T_i}{e}\left|\frac{e\delta\phi_0}{T_i}\right|^2\frac{e\delta\phi_Z}{T_i}$$

and from equation (13) there is:

$$\hat{\chi}_{iZ}\partial_t\delta\phi_Z = \gamma_2|\delta\phi_0|^2 - \nu_{ii}\delta\phi_Z$$
$$\frac{1}{\omega_A}\partial_t\frac{e\delta\phi_Z}{T_i} = \frac{\gamma_2}{\hat{\chi}_{iZ}\omega_A}\frac{T_i}{e}\left|\frac{e\delta\phi_0}{T_i}\right|^2 - \frac{\nu_{ii}}{\hat{\chi}_{iZ}\omega_A}\frac{e\delta\phi_Z}{T_i}.$$

Then,

$$\partial_\tau x = \hat{\gamma}_1 x - \hat{\gamma}_d xy \tag{A26}$$

$$\partial_\tau y = \hat{\gamma}_2 x - \hat{\nu}_{ii}y \tag{A27}$$

where $\tau\equiv\omega_A t$, $x\equiv\left|\frac{e\delta\phi_0}{T_i}\right|^2$, $y\equiv\frac{e\delta\phi_Z}{T_i}$ and notice

$$\Omega_{*E} = \frac{cT_i}{eB_0}k_\theta L^{-1}_{n_{0E}} = D_B k_\theta L^{-1}_{n_{0E}},$$
$$D_B\equiv\frac{cT_i}{eB_0},\quad \hat{\chi}_{iZ}\sim 1.6\frac{q^2}{\sqrt{\varepsilon}}$$

therefore,

$$\hat{\gamma}_1\equiv\frac{\gamma_1}{\omega_A} = \frac{\pi}{2\sigma}q^3k_{\theta,0}\rho_A\beta_E f_r\frac{R_0}{L_{n0E}}$$
$$\hat{\gamma}_d\equiv\frac{\gamma_d}{\omega_A}\frac{T_i}{e} = \frac{2c}{B_0}k_{\theta,0}k_Z\frac{T_i}{e}\frac{1}{\omega_A} = \frac{2D_B k_{\theta,0}k_Z}{\omega_A}$$
$$\hat{\gamma}_2\equiv\frac{\gamma_2}{\hat{\chi}_{iZ}\omega_A}\frac{T_i}{e}\simeq\frac{cT_i}{B_0 e}\frac{k_{\theta,0}\hat{F}\varepsilon}{\hat{\chi}_{iZ}\omega_A} = \frac{D_B k_{\theta,0}\hat{F}\varepsilon}{\hat{\chi}_{iZ}\omega_A}\simeq\frac{\hat{\gamma}_d}{2}$$
$$\hat{\nu}_{ii}\equiv\frac{\nu_{ii}}{\hat{\chi}_{iZ}\omega_A}.$$

The effective collisionless damping ν_G can be incorporated into the expression $\hat{\nu}=(\nu_{ii}+\nu_G)/(\hat{\chi}_{iZ}\omega_A)$. Using equations (A26) and (A27), and decomposing the quantities into their saturated and fluctuating components $x=x_0+\tilde{x}$, $y=y_0+\tilde{y}$, we can analyze the linear instabilities of this system

$$\partial_\tau\tilde{x} = \hat{\gamma}_1\tilde{x} - \hat{\gamma}_d x_0\tilde{y} - \hat{\gamma}_d\tilde{x}y_0 \tag{A28}$$

$$\partial_\tau \tilde{y} = \hat{\gamma}_2 \tilde{x} - \hat{\nu}_{ii} \tilde{y}. \tag{A29}$$

Here $x_0 = y_0 \hat{\nu}_{ii}/\hat{\gamma}_2$, $y_0 = \hat{\gamma}_1/\hat{\gamma}_d$. The above system has two eigenvalues $\lambda_{1,2}$:

$$\lambda_{1,2} = -\frac{1}{2}\left[\hat{\nu}_{ii} \pm \sqrt{\hat{\nu}_{ii}\left(\hat{\nu}_{ii} - 4\hat{\gamma}_1\right)}\right]. \tag{A30}$$

When $\hat{\nu}_{ii} < 4\hat{\gamma}_1$, i.e. the damping of ZM is smaller than the growth of TAE $\nu_{ii} \lesssim \gamma_{\rm TAE}$, the system will experience oscillatory decay to saturation states. The oscillation rate is determined from the imaginary part of eigenvalue $|\Im\lambda_{1,2}| = \sqrt{\hat{\nu}_{ii}(4\hat{\gamma}_1 - \hat{\nu}_{ii})}/2$, which is approximately $f_{\rm osc} \sim \sqrt{\nu_{ii}\gamma_1}/\omega_A$.

Appendix B. Geodesic acoustic transference

Here we introduce a simple generalization of geodesic acoustic transference [39–41]. The evolution of ZF can be expressed as:

$$\partial_t \langle \tilde{u} \rangle_Z = \gamma_Z \langle \tilde{u} \rangle_Z - \omega_B \langle p_s \sin\vartheta \rangle_Z \tag{B1}$$

where $\langle \tilde{u} \rangle_Z$ is the ZF, ϑ is the poloidal angle, p_s is the sideband pressure with $(m = 1, n = 0)$, γ_Z represents the drive of ZF, $\omega_B \equiv 2L_\perp/R$ is geodesic CCT from thermal plasma. The evolution of electron pressure sideband can be expressed as:

$$\begin{aligned}\partial_t \langle p_{e,s} \sin\vartheta \rangle_Z =& -\partial_x \langle \tilde{p}_e \tilde{v}_E^x \sin\vartheta \rangle_Z + \langle v_\parallel \cos\vartheta \rangle_Z \\ & - \frac{\omega_B}{2}\langle (\partial_x p - \tilde{u}) \rangle_Z \\ \simeq & -\frac{D_{\rm turb}}{L_\perp^2}\langle p_{e,s} \sin\vartheta \rangle_Z + \langle u_\parallel \cos\vartheta \rangle_Z \\ & - \langle J_\parallel \cos\vartheta \rangle_Z - \frac{\omega_B}{2}\langle \partial_x p \rangle_Z + \frac{\omega_B}{2}\langle \tilde{u} \rangle_Z\end{aligned}$$

where the magnetic flutter effect is neglected, quasilinear turbulent coefficient is assumed, $L_\perp$ is the perpendicular profile scale of thermals. The ion flow sideband $\langle u_\parallel \cos\vartheta \rangle_Z$ is typically small, current sideband and diamagnetic part cancel each other out. Then the evolution of pressure sideband is:

$$\partial_t \langle p_{e,s} \sin\vartheta \rangle_Z = -\frac{D_{\rm turb}}{L_\perp^2}\langle p_{e,s} \sin\vartheta \rangle_Z + \frac{\omega_B}{2}\langle \tilde{u} \rangle_Z. \tag{B2}$$

Here we consider the simple case of damping through turbulent mixing and define $\tau_{\rm turb}^{-1} \equiv (D_{\rm turb}/L_\perp^2)$, $D_{\rm turb} \simeq {\rm Re}\sum_{\tilde{\mathbf{k}}} i\frac{c^2}{B_0^2}|\phi_{\tilde{\mathbf{k}}}|^2/(\omega - \tilde{\mathbf{k}}_\perp \cdot \mathbf{v}_E)$, $\tilde{\mathbf{k}}_\perp$ refers to thermal plasma turbulent wave number.

Dedimensionalizing the above equation, combining with the evolution system of ZF and TAE, we arrive at equations (18)–(20):

$$\partial_\tau x = \hat{\gamma}_1 x - \hat{\gamma}_d x y \tag{B3}$$

$$\partial_\tau y = \hat{\gamma}_2 x - \hat{\nu}_{ii} y - \frac{C_S^2 q R_0}{i k_Z D_B \hat{\chi}_{iZ} \omega_A L_\perp^2}\omega_B z \tag{B4}$$

$$\partial_\tau z = (1+\tau_i)\frac{i k_Z D_B}{V_A}\frac{\omega_B}{2} y - \frac{1}{\omega_A \tau_{\rm turb}} z \tag{B5}$$

where $z \equiv \langle p_s \sin\vartheta \rangle_Z = (1+\tau_i)\langle p_{e,s} \sin\vartheta \rangle_Z$. It's easy to notice the geodesic acoustic oscillation:

$$\frac{2(1+\tau_i)C_S^2/R^2}{\hat{\chi}_{iZ}\omega_A^2} = \frac{1}{\hat{\chi}_{iZ}}\frac{\omega_{\rm GAM}^2}{\omega_A^2}. \tag{B6}$$

For the static sideband, there is

$$z_{\rm static} = (1+\tau_i)\frac{i k_Z D_B}{V_A}\frac{\omega_B}{2}\omega_A \tau_{\rm turb} y.$$

Then the damping rate caused by geodesic acoustic transference is:

$$\begin{aligned}\hat{\nu}_G &= \frac{C_S^2 q R_0}{i k_Z D_B \hat{\chi}_{iZ} \omega_A L_\perp^2}\omega_B z_{\rm static} \\ &= \frac{1}{\chi_{iZ}}\frac{\omega_{\rm GAM}^2}{\omega_A \tau_{\rm turb}^{-1}}\end{aligned} \tag{B7}$$

where $\omega_{\rm GAM}^2 \equiv 2(1+\tau_i)C_S^2/R^2 = 2q\omega_A^2\sqrt{\beta_{\rm bulk}}$. In the evolution of ZF, we can write down:

$$\partial_\tau y = \hat{\gamma}_2 x - \hat{\nu}_{ii} y - \hat{\nu}_G y. \tag{B8}$$

With $\omega_A \sim 10^6\,{\rm rad\,s^{-1}}$, $\omega_{\rm GAM} \sim 10^5\,{\rm rad\,s^{-1}}$, and $\tau_{\rm turb}^{-1} = D_{\rm turb}/L_\perp^2 \sim 10^5\,{\rm Hz}$, we have:

$$\hat{\nu}_G \sim \mathcal{O}\left(10^{-2}\right) - \mathcal{O}\left(10^{-1}\right). \tag{B9}$$

Appendix C. The parameters used to generate figures 2, 3

We used a combination of DIII-D parameters and profiles similar to those in figure 1 of [20], as listed in table 1. The derived parameters used to generate figures 2, 3, and other estimates are provided in table 2. Note that the 2π factor is neglected in all frequency calculations.

Table 1. The parameters are based on the DIII-D device and the EP profile in [20].

R_0	1.75	m
a	0.64	m
ε	a/R_0	1
L_{n0E}	$0.5a$	m
$L_\perp$	$0.9a$	m
B_0	20	kGs
n_0	3×10^{13}	cm^{-3}
T_{ev}	2×10^{3}	eV
f_β	1	1
τ	1	1
n	4	1
m	6	1
q	$(m+1/2)/n$	1
c	3×10^{10}	$\mathrm{cm\,s}^{-1}$
e	4.8×10^{-10}	esu
V_f/V_A	1.2	1

Table 2. A series of parameters derived from table 1, used for figures 2, 3 and estimates in the paper. Note that the 2π factor is neglected in all frequency calculations.

ρ_i	0.0031 305	m
Ω_i	3.04845×10^{7}	1/s
$k_\perp=0.5\epsilon/\rho_i$	58.4116	1/m
$k_{\theta 0}$	10.1563	1/m
$k_Z=k_\perp/4$	14.6029	1/m
f_β	1	1
f_r	0.25	1
β_{bulk}	0.0120 697	1
$\sigma=\left(\frac{V_f}{V_A}\right)^2\log\left(\left(\frac{V_f}{0.5V_A}\right)^2\right)$	2.5	1
D_B	1000.	$\mathrm{m^2\,s^{-1}}$
V_A	8.03326×10^{6}	$\mathrm{m\,s^{-1}}$
C_s	$200000\sqrt{5}$	$\mathrm{m\,s^{-1}}$
ω_A	2.82488×10^{6}	1/s
ω_{GAM}	511 101.	1/s
Ω_{*E}/ω_A	0.0112 353	1
ν_{ii}	391.284	1/s
ν_{total}	2.04839×10^{6}	1/s
ω_{ExB}	210 204.	1/s
$\omega_{\mathrm{ExB}}a/C_s$	0.300 819	1
$\Omega_Z=k_{\theta 0}V_{\mathrm{ExB}}$	18 274.5	1/s
$(\delta B_r/B_0)^2$	$2.22057578350852\times10^{-7}$	1
$\mathrm{TAE}_{\mathrm{sat/th}}$	0.268 055	1
$\hat{\gamma}_1$	0.118 065	1
$\hat{\gamma}_d$	0.105 003	1
$\hat{\gamma}_2$	0.0525 015	1
$\hat{\nu}_{ii}$	0.00 001 9826	1
$\hat{\nu}_G$	0.10 377	1
$\hat{\gamma}_{\mathrm{G1}}$	$-3.91558i$	1
$\hat{\gamma}_{\mathrm{G2}}$	$+0.00119663i$	1
$\hat{\gamma}_3$	0.0451 527	1
$1/\tau_{\mathrm{turb}}$	127 551.	1/s
$1/(\omega_A\tau_{\mathrm{turb}})$	0.0451 527	1
$3\hat{\gamma}_d\hat{\gamma}_2-(\omega_A\tau_{\mathrm{turb}})^{-2}$	0.0144 997	1
$\tau_Z/\tau_{\mathrm{turb}}$	0.860 026	1
f_{osc}	0.110 698	$1/\omega_A$
$(f_r f_\beta)_{\mathrm{crit}}$	0.0831 064	1

ORCID iDs

Qinghao Yan 0000-0002-2541-8089
P.H. Diamond 0000-0003-3273-2604

References

[1] Chen L. and Zonca F. 2016 Physics of Alfvén waves and energetic particles in burning plasmas *Rev. Mod. Phys.* **88** 015008
[2] Di Siena A. *et al* 2021 New high-confinement regime with fast ions in the core of fusion plasmas *Phys. Rev. Lett.* **127** 025002
[3] Han H. *et al* 2022 A sustained high-temperature fusion plasma regime facilitated by fast ions *Nature* **609** 269–75
[4] Mazzi S. *et al* (JET Contributors) 2022 Enhanced performance in fusion plasmas through turbulence suppression by megaelectronvolt ions *Nat. Phys.* **18** 776–82
[5] Citrin J. and Mantica P. 2023 Overview of tokamak turbulence stabilization by fast ions *Plasma Phys. Control. Fusion* **65** 033001
[6] Garcia J. *et al* 2024 Stable Deuterium-Tritium plasmas with improved confinement in the presence of energetic-ion instabilities *Nat. Commun.* **15** 7846
[7] Hahm T.S., Choi G.J., Park S.J. and Na Y.-S. 2023 Fast ion effects on zonal flow generation: a simple model *Phys. Plasmas* **30** 072501
[8] Choi G.J., Diamond P.H. and Hahm T.S. 2023 On how fast ions enhance the regulation of drift wave turbulence by zonal flows *Nucl. Fusion* **64** 016029
[9] Romanelli M., Zocco A. and Crisanti F. (JET-EFDA Contributors) 2010 Fast ion stabilization of the ion temperature gradient driven modes in the Joint European Torus hybrid-scenario plasmas: a trigger mechanism for internal transport barrier formation *Plasma Phys. Control. Fusion* **52** 045007
[10] Zhang H. and Lin Z. 2013 Nonlinear generation of zonal fields by the beta-induced Alfvén Eigenmode in tokamak *Plasma Sci. Technol.* **15** 969–73
[11] Spong D.A., Van Zeeland M.A., Heidbrink W.W., Du X., Varela J., Garcia L. and Ghai Y. 2021 Nonlinear dynamics and transport driven by energetic particle instabilities using a gyro-Landau closure model *Nucl. Fusion* **61** 116061
[12] Mazzi S., Garcia J., Ye D.Z. Kazakov O., Ongena J., Dreval M., Nocente M., Štancar Ž and Szepesi G. (JET Contributors) 2022 Gyrokinetic study of transport suppression in JET plasmas with MeV-ions and toroidal Alfvén eigenmodes *Plasma Phys. Control. Fusion* **64** 114001
[13] Di Siena A., Görler T., Poli E., Bañón Navarro A., Biancalani A. and Jenko F. 2019 Electromagnetic turbulence suppression by energetic particle driven modes *Nucl. Fusion* **59** 124001
[14] Brochard G. *et al* 2024 Saturation of fishbone instability by self- generated zonal flows in tokamak plasmas *Phys. Rev. Lett.* **132** 075101
[15] Diamond P.H., Itoh S.I., Itoh K. and Hahm T.S. 2005 Zonal flows in plasma—a review *Plasma Phys. Control. Fusion* **47** R35–R161
[16] Chen L. and Zonca F. 2012 Nonlinear excitations of zonal structures by Toroidal Alfvén eigenmodes *Phys. Rev. Lett.* **109** 145002
[17] Diamond P.H. and Kim Y.-B. 1991 Theory of mean poloidal flow generation by turbulence *Phys. Fluids B* **3** 1626–33
[18] Qiu Z., Chen L. and Zonca F. 2016 Effects of energetic particles on zonal flow generation by toroidal Alfvén eigenmode *Phys. Plasmas* **23** 090702
[19] Qiu Z., Chen L. and Zonca F. 2017 Nonlinear excitation of finite-radial-scale zonal structures by toroidal Alfvén eigenmode *Nucl. Fusion* **57** 056017
[20] Todo Y., Berk H.L. and Breizman B.N. 2010 Nonlinear magnetohydrodynamic effects on Alfvén eigenmode evolution and zonal flow generation *Nucl. Fusion* **50** 084016
[21] Chen Y., Fu G.Y., Collins C., Taimourzadeh S. and Parker S.E. 2018 Zonal structure effect on the nonlinear saturation of reverse shear Alfven eigenmodes *Phys. Plasmas* **25** 032304
[22] Qiu Z., Chen L. and Zonca F. 2023 Gyrokinetic theory of toroidal Alfvén eigenmode saturation via nonlinear wave-wave coupling *Rev. Mod. Plasma Phys.* **7** 28
[23] Falessi M.V., Chen L., Qiu Z. and Zonca F. 2023 Nonlinear equilibria and transport processes in burning plasmas *New J. Phys.* **25** 123035
[24] Biancalani A., Bottino A., Lauber P., Mishchenko A. and Vannini F. 2020 Effect of the electron redistribution on the nonlinear saturation of Alfvén eigenmodes and the excitation of zonal flows *J. Plasma Phys.* **86** 825860301
[25] Biancalani A. *et al* 2021 Gyrokinetic investigation of Alfvén instabilities in the presence of turbulence *Plasma Phys. Control. Fusion* **63** 065009
[26] Liu Z. and Fu G. 2023 A simple model for internal transport barrier induced by fishbone in tokamak plasmas *J. Plasma Phys.* **89** 905890612
[27] Chen L., Qiu Z. and Zonca F. 2022 On scattering and damping of toroidal Alfvén eigenmode by drift wave turbulence *Nucl. Fusion* **62** 094001
[28] Zonca F. and Chen L. 2014 Theory on excitations of drift Alfvén waves by energetic particles. I. Variational formulation *Phys. Plasmas* **21** 072120
[29] Zonca F., Chen L., Briguglio S., Fogaccia G., Vlad G. and Wang X. 2015 Nonlinear dynamics of phase space zonal structures and energetic particle physics in fusion plasmas *New J. Phys.* **17** 013052
[30] Fu G.Y. and Cheng C.Z. 1992 Excitation of high-n toroidicity-induced shear Alfvén eigenmodes by energetic particles and fusion alpha particles in tokamaks *Phys. Fluids B* **4** 3722–34
[31] Biglari H., Zonca F. and Chen L. 1992 On resonant destabilization of toroidal Alfvén eigenmodes by circulating and trapped energetic ions/alpha particles in tokamaks *Phys. Fluids B* **4** 2385–8
[32] Chen L., Lin Z., White R.B. and Zonca F. 2001 Non-linear zonal dynamics of drift and drift-Alfvén turbulence in tokamak plasmas *Nucl. Fusion* **41** 747
[33] Rosenbluth M.N. and Hinton F.L. 1998 Poloidal flow driven by ion-temperature-gradient turbulence in Tokamaks *Phys. Rev. Lett.* **80** 724–7
[34] Qiu Z., Chen L. and Zonca F. 2019 Gyrokinetic theory of the nonlinear saturation of a toroidal Alfvén eigenmode *Nucl. Fusion* **59** 066024
[35] Falessi M.V. and Zonca F. 2019 Transport theory of phase space zonal structures *Phys. Plasmas* **26** 022305
[36] Diamond P.H., Liang Y.-M., Carreras B.A. and Terry P.W. 1994 Self-regulating shear flow turbulence: a paradigm for the L to H Transition *Phys. Rev. Lett.* **72** 2565–8
[37] Berk H.L., Breizman B.N. and Huanchun Y. 1992 Scenarios for the nonlinear evolution of alpha-particle-induced Alfvén wave instability *Phys. Rev. Lett.* **68** 3563–6
[38] Lesur M. 2010 The Berk-Breizman model as a paradigm for energetic particle-driven Alfvén Eigenmodes *PhD Thesis* École Polytechnique (available at: www.researchgate.net/publication/48907493_The_Berk-Breizman_Model_as_a_Paradigm_for_Energetic_Particle-driven_Alfven_Eigenmodes)
[39] Scott B. 1997 Three-dimensional computation of drift Alfvén turbulence *Plasma Phys. Control. Fusion* **39** 1635–68

[40] Scott B. 2003 The geodesic transfer effect on zonal flows in tokamak edge turbulence *Phys. Lett. A* **320** 53–62
[41] Scott B. 2005 Energetics of the interaction between electromagnetic ExB turbulence and zonal flows *New J. Phys.* **7** 92–92
[42] Wang S. 2017 Zonal flows driven by the turbulent energy flux and the turbulent toroidal Reynolds stress in a magnetic fusion torus *Phys. Plasmas* **24** 102508
[43] Wang Z., Dai Z. and Wang S. 2022 Nonlinear excitation of zonal flows by turbulent energy flux *Phys. Rev. E* **106** 035205
[44] Chen L., Qiu Z. and Zonca F. 2024 On beat-driven and spontaneous excitations of zonal flows by drift waves *Phys. Plasmas* **31** 040701
[45] Ajay C.J., Brunner S., McMillan B., Ball J., Dominski J. and Merlo G. 2020 How eigenmode self-interaction affects zonal flows and convergence of tokamak core turbulence with toroidal system size *J. Plasma Phys.* **86** 905860504
[46] Diamond P.H. *et al* 2001 Secondary instability in drift wave turbulence as a mechanism for zonal flow and avalanche formation *Nucl. Fusion* **41** 1067
[47] Lin W.H., Garcia J., Li J.Q., Mazzi S., Li Z.J., He X.X. and Yu X. 2023 A self-sustaining mechanism for internal transport barrier formation in HL-2A tokamak plasmas *Nucl. Fusion* **63** 126048
[48] Kim D. *et al* 2023 Turbulence stabilization in tokamak plasmas with high population of fast ions *Nucl. Fusion* **63** 124001
[49] Dif-Pradalier G. *et al* 2015 Finding the elusive E×B staircase in magnetized plasmas *Phys. Rev. Lett.* **114** 085004
[50] Qinghao Y. and Diamond. P.H. 2022 Staircase formation by resonant and non-resonant transport of potential vorticity *Nucl. Fusion* **62** 126032
[51] Kosuga Y., Diamond P.H. and Gürcan O..D. 2010 On the efficiency of intrinsic rotation generation in tokamaks *Phys. Plasmas* **17** 102313
[52] Ida K. *et al* 2010 Spontaneous toroidal rotation driven by the off-diagonal term of momentum and heat transport in the plasma with the ion internal transport barrier in LHD *Nucl. Fusion* **50** 064007
[53] Fiore C.L. *et al* 2012 Production of internal transport barriers via self-generated mean flows in Alcator C-Mod *Phys. Plasmas* **19** 056113
[54] Diamond P.H. *et al* 2013 An overview of intrinsic torque and momentum transport bifurcations in toroidal plasmas *Nucl. Fusion* **53** 104019
[55] Ruiz Ruiz J. the JET Contributors and the EUROfusion Tokamak Exploitation Team *et al* 2025 Measurement of zero-frequency fluctuations generated by coupling between Alfvén modes in the JET Tokamak *Phys. Rev. Lett.* **134** 095103
[56] Li J.C. and Diamond P.H. 2018 Another look at zonal flows: resonance, shearing and frictionless saturation *Phys. Plasmas* **25** 042113
[57] John W.M. 1961 On the stability of heterogeneous shear flows *J. Fluid Mech.* **10** 496–508
[58] Louis N.H. 1961 Note on a paper of John W. Miles *J. Fluid Mech.* **10** 509–12
[59] Fu G.Y. and Park W. 1995 Nonlinear hybrid simulation of the toroidicity-induced Alfvén eigenmode *Phys. Rev. Lett.* **74** 1594–6
[60] Todo Y., Sato T., Watanabe K., Watanabe T.H. and Horiuchi R. 1995 Magnetohydrodynamic Vlasov simulation of the toroidal Alfvén eigenmode *Phys. Plasmas* **2** 2711–6
[61] Briguglio S., Zonca F. and Vlad G. 1998 Hybrid magnetohydrodynamic-particle simulation of linear and nonlinear evolution of Alfvén modes in tokamaks *Phys. Plasmas* **5** 3287–301
[62] Lang J. and Guo-Yong F. 2011 Nonlinear simulation of toroidal Alfvén eigenmode with microturbulence-induced radial diffusion *Phys. Plasmas* **18** 055902
[63] Lilley M.K., Breizman B.N. and Sharapov S.E. 2010 Effect of dynamical friction on nonlinear energetic particle modes *Phys. Plasmas* **17** 092305
[64] Duarte V.N., Berk H.L., Gorelenkov N.N., Heidbrink W.W., Kramer G.J., Nazikian R., Pace D.C., Podestà M. and Van Zeeland M.A. 2017 Theory and observation of the onset of nonlinear structures due to eigenmode destabilization by fast ions in tokamaks *Phys. Plasmas* **24** 122508
[65] Liu P., Wei X., Lin Z., Heidbrink W.W., Brochard G., Choi G.J., Nicolau J.H. and Zhang W. 2024 Cross-scale interaction between microturbulence and meso-scale reversed shear Alfvén eigenmodes in DIII-D plasmas *Nucl. Fusion* **64** 076007